The LWA-1 S60 System

S. Ellingson,[*] Q. Liu,[†] and J. Craig[‡]

Dec 21, 2010 (v.2)

Contents

---

[*]Virginia Tech, `ellingson@vt.edu`
[†]Virginia Tech, `qianliu@vt.edu`
[‡]U. New Mexico, `joecraig@unm.edu`

1   Introduction

This report documents the "LWA-S60" system that was installed on the first station of the Long Wavelength Array (LWA-1) between January 2010 and October 2010. The purpose of the system was to provide data acquisition, including beamforming, in the interim period between the initial availability of the LWA-1 analog subsystems (antennas through analog receivers), which became available for a small number of antennas in Fall 2009; and the digital processing (DP) subsystem, which is currently still in development. The various configurations of the system used up to 30 dipoles, with analog delay-and-sum beamforming and FPGA evaluation boards in lieu of the DP subsystem. The FPGA evaluation boards and firmware had previously been purchased and developed, respectively, for future use in ETA[1], and so were available for immediate use in this system. The term "S60" refers to the part number of the FPGA used in the evaluation board[2], and is also the informal term we use to refer to the FPGA boards.

The LWA-S60 system existed in two distinct versions. The first version of the system, which we shall refer to as "S60-1", was operational between January 2010 and July 2010, used up to 8 dipoles at a time, and produced an instantaneous bandwidth of 3.58 MHz (3 dB). The second version of the system, which we shall refer to as "S60-2", was operational between July 2010 and October 2010, used up to 30 dipoles at a time, and produced an instantaneous bandwidth of 1.86 MHz (3 dB). Both S60-1 and S60-2 were capable of observing at two separate frequencies simultaneously, but the S60-2 version was capable of capturing beam data simultaneously with data from an outrigger dipole on both frequencies; i.e., both signals at both frequencies. Sensitivity on the order of 20 Jy (5 σ, 1.86 MHz, 103 s) was achieved by S60-2 with a 30-dipole beam (see Sections 4.2 and 4.3, in particular Tables 4 and 5, for details). Most (but not all) of the data was collected at frequencies around 38 MHz and 74 MHz. From the archived raw data, integration times ranging from 400 ns to hours are possible, and we show in Section 3 evidence that noise-limited integrations up to 1 h are possible with only moderate frequency blanking. A total of about 366 h of useful observation was conducted using S60-1 and S60-2, with an additional 506 h of useful long-duration "low duty cycle" observations also available; see Appendix C for details. A total of 17.5 TB of data has been recorded, documented, and archived.

Although science analysis has not yet begun in earnest, we anticipate that this data will be most useful for surveys/searches of transient astrophysical phenomena over a wide range of time scales, and possibly also for pulsar studies, including Crab giant pulses. The data may also be useful for studies of radio frequency interference. Finally, the analysis documented in Section 4 may be useful as a template for a similar procedure used as part of the commissioning process for the completed LWA-1 station; in particular, validating the DP beamforming mode once it becomes operational.

The remainder of this report is organized as follows. The design of the S60-1 and S60-2 versions of the LWA-S60 is documented in Section 2. Section 3 shows some initial results using data captured from the system. An assessment of the system characteristics, including sensitivity and beam shape, is provided in Section 4. Although it is very difficult to precisely verify these estimates using observations, we demonstrate in Section 4 that out estimates are at least consistent with acquired data. Appendix C summarizes the observation datasets obtained with the S60-1 and -2 systems.

---

[1]`http://www.ece.vt.edu/swe/eta/`

[2]The board uses the Altera Stratix II EP2S60F1020C4 FPGA; those familiar with the arcana of Altera part numbering schemes and the history of their use in evaluation boards might know why "S60" turns out to be a convenient nickname.

2   System Description

The S60-1 and S60-2 systems use LWA-1 production hardware from analog receivers ("ARXs" in LWA-speak) skyward. A summary of components is given below with references to the most applicable source of additional information:

- *Antennas*: LWA antennas are organized into "stands". A stand is defined as two dipole-type antennas, connected to a "front end electronics" (FEE) unit, held up by a mast. A concise summary of the stand design, minus the FEE, can be found in Section III-A of [1]. The two antennas of a stand are oriented such that one is aligned North-South (henceforth, "NS"), and the other is East-West (henceforth "EW").[3]

- *FEE*: This device serves as both a 2:1 balun and also sets the system-internal contribution to the system temperature of approximately 300 K. The design is documented in [2].

- *Array geometry and cabling*: The array geometry and details of the system of cables that connect stands to ARXs are documented in [3]. Stands numbered 1 though 257 are clustered together with minimum mast-to-mast spacing of 5 m. Stand 258 is a standalone "outrigger" located roughly 300 m east of the center of this array. The LWA-S60 system used the EW-oriented dipoles of the main array and the NS-oriented dipole of Stand 258.

- *ARX*: These provide gain and provide the first stage of analog bandwidth limiting. The ARX design is documented in [4]. The outputs of the production ARXs are differential; for the LWA-S60 system these were converted from differential to single-ended using multichannel "balun boards" which are not part of the LWA-1 system.

- *Analog Beamformer*: In all versions of the LWA1-S60 system, dipoles are either digitized directly, or combined through a system of delay lines and RF power combiners. To implement beamforming delays, we used various combinations of RG-58 coaxial cable plus Stanford Research Systems Model DB64 switch-programmable delay line units, which allow 0 to 63.5 ns delays in steps of 0.5 ns. In each of the major versions of the system (S60-1 and S60-2, as identified in Section 1), several configurations were employed. Here is a summary of these configurations:

  - *S60-1a* (January 8–11, 2010): No beamformer. Looking at test signals and conducting commissioning observations using individual dipoles. Observations were made using Stands 112, 119, 189, 214, and 228 (individually) at center frequencies of 33.25 MHz, 36.75 MHz, and 50.75 MHz.

  - *S60-1x and S60-1y* (January 11 – February 24, 2010): 7-dipole beamformer, using one FPGA board to observe at either 36.75 MHz, and the other to observe at 33.25 MHz or 50.75 MHz. The beam was pointed south at a zenith angle of either 36° (S60-1x) or 22° (S60-1y). These configurations are essentially the same as S60-1b (see below), but we identify the associated observations separately because one of the dipoles was phase-reversed due to a wiring error in the balun interface board following the ARX output during this period.

  - *S60-1b* (March 24–29, 2010): 8-dipole beamformer, using one FPGA board to observe at 22.75 MHz and the other to observe at 72.75 MHz. The beam was pointed south at a zenith angle of 22°. See Figures 1, 2, and 3.

  - *S60-1c* (April 4 – May 13, 2010): One FPGA was used to observe the output of the 8-dipole beamformer at 72.75 MHz (same as S60-1b), and the other was used to observe a single dipole (Stand 15) at the same frequency. See Figures 1, 2, and 4.

---

[3]To be clear, here we are referring to the orientation of the E-plane of the dipole.

– *S60-2a* (July 11, 12, and 16): Simultaneous observations of dipoles on Stands 230 and 258. One FPGA was used to observe both dipoles at 74.56 MHz, the other was used to do the same at 38.00 MHz.

– *S60-2b* (July 13, 2010): Simultaneous observations of a 17-dipole beam pointed north at zenith angle 24.8°, and a dipole from Stand 258. One FPGA was used to observe both outputs at 74.56 MHz, the other was used to do the same at 38.00 MHz. See Figures 5, 6, 7; and Table 1.

– *S60-2c* (July 15–22, 2010): Same as S60-2b, except now using either 26 or 30 dipoles to form the beam. See Figures 5, 6, 7; and Table 2.

– *S60-2d* (July 22–October 13, 2010): Same as S60-2c, except the beam pointed is pointed south at zenith angle 12°. See Figures 6 and 7; and Table 3. The stands used in this configuration are shown in Figure 8.

- *FPGA Boards:* We used Altera "DSP Development Kit, Stratix II Edition" FPGA development boards, which we commonly refer to as "S60 boards" (again, a reference to the part number of the FPGA chip used). These are shown in Figures 2(b) and 6(b). Each S60 board includes a pair of 12-bit 120 MSPS analog-to-digital converters connected to the FPGA, which is in turn connected to a 100BaseT Ethernet output. The output sample format is 7 bits "I" plus 7 bits "Q". Samples are collected into packets which are output as a UDP data stream. Details of the board and the firmware we developed for it are available in design reports available separately; there is one for the S60-1 system [5] and one for the S60-2 system [6]. The primary differences between the two are that the S60-1 firmware accepts input from only one A/D and has an output bandwidth of 3.58 MHz (3 dB); whereas the S60-2 firmware accepts input from both A/Ds and provides outputs associated with both, multiplexed together, each having bandwidth 1.86 MHz (3 dB). The employment of these boards in each system is illustrated in Figures 3, 4, and 7. A subtle difference between the two firmware versions is that the S60-1 firmware uses a high-order CIC filter, whereas the S60-2 firmware uses traditional multirate FIR filters. As the former has a fast, small ripple in the frequency response, the latter is easier to work with if precise bandpass calibration is desired.

- *Data Recorder PCs*: The Ethernet output of each FPGA board is captured by a custom-built mini-ITX-form-factor PC, shown in Figures 2(b) and 6(b), running Ubuntu Linux 9.04. These PCs are sometimes referred to by the hostnames "k1" and "k2". Data is captured using a Python script. Usually, the data is divided into 980 MB files, each representing either 140 s (S60-1) or 103 s (S60-2) of continuous observation. Bash scripts are used to iteratively run the Python capture program for nearly-continuous data capture, with only very brief gaps ($\ll 1$ s) between files. Typically, an observation consists of 100 files, which is about 3.9 h (S60-1) or 2.9 h (S60-2) of observation, corresponding to about 96 GB of data.

Additional details about the S60-1 version of the LWA1-S60 system are available in a report written in January 2010, shortly following the installation and commissioning of that system; see [7].
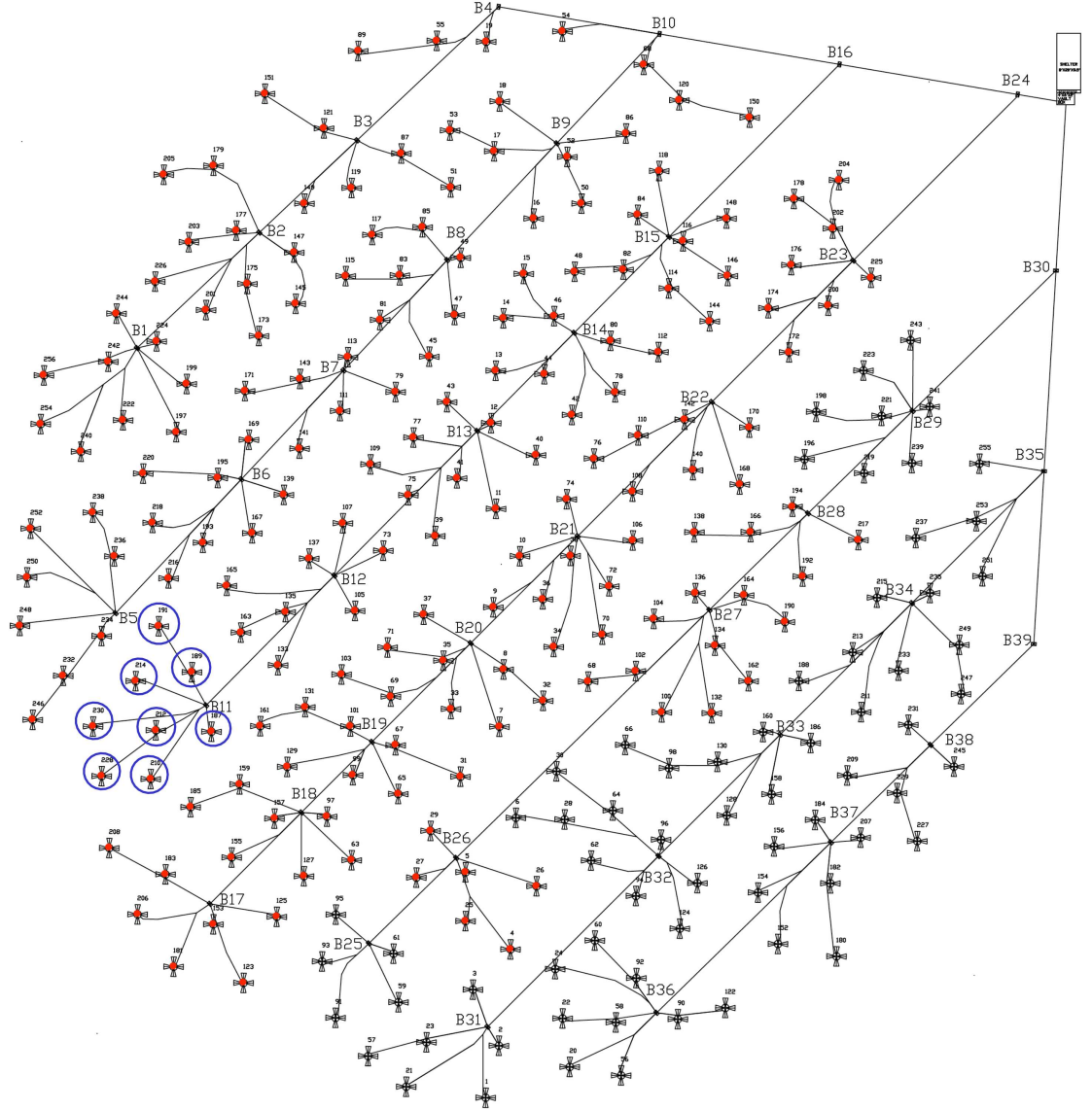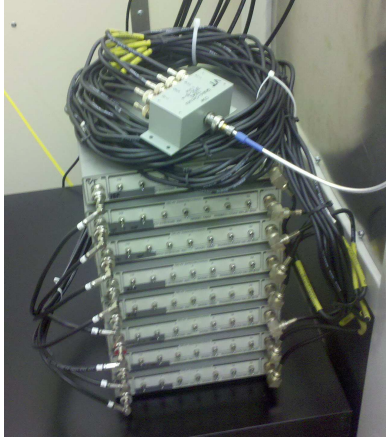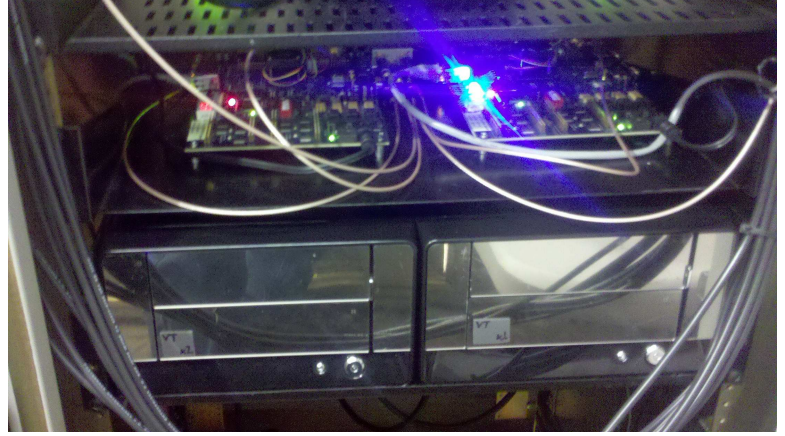
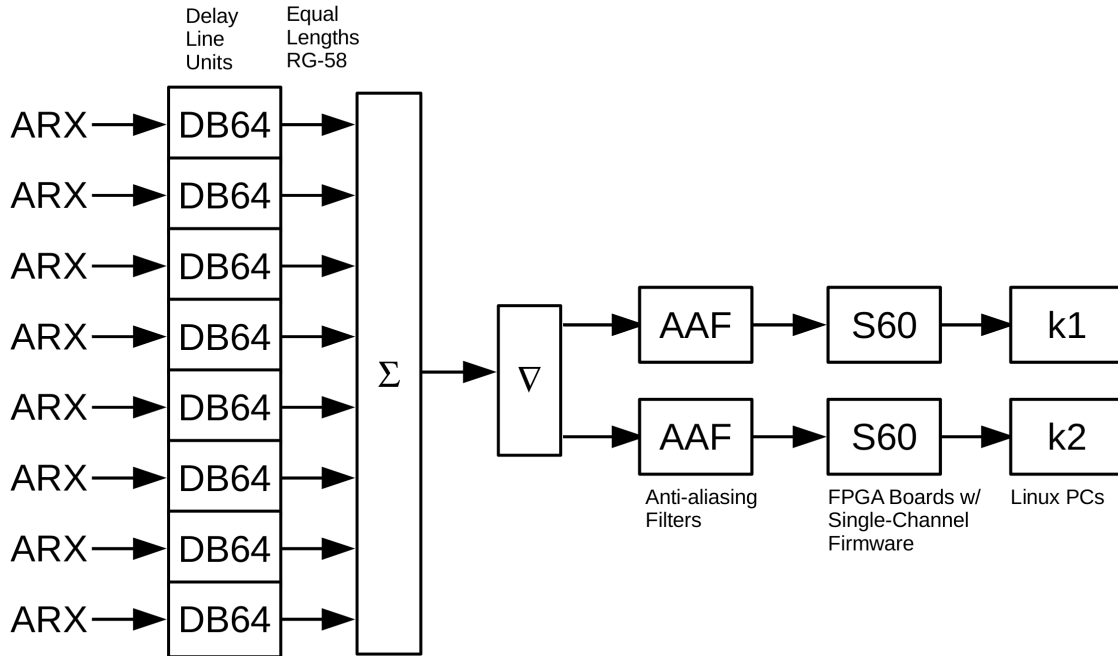Figure 1: Stands used in the S60-1 beamformers. Stand 187 was not used in the S60-1x and -1y configurations.
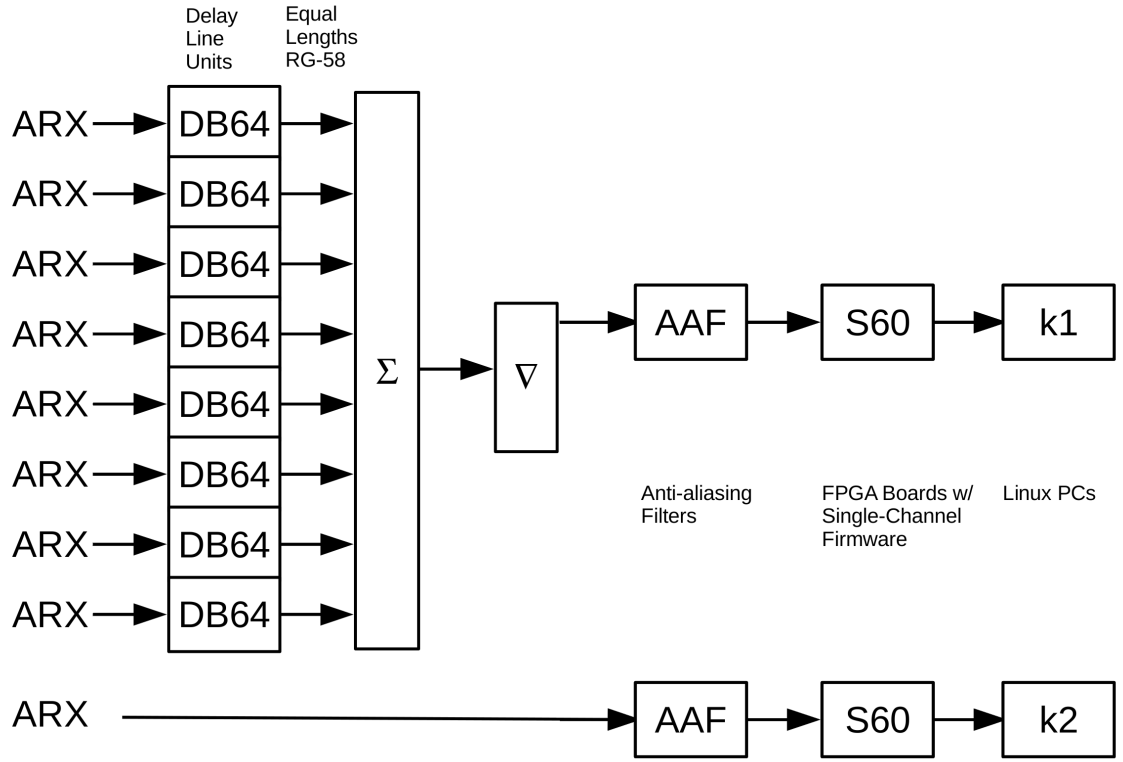
(a) analog beamformer (b) FPGA boards ("S60s") and PCs ("k1" & "k2")

Figure 2: Components of the S60-1 system.

Configuration	187	189	191	210	212	214	228	230
S60-1b	38.5 ns	26.0 ns	3.0 ns	11.0 ns	27.5 ns	12.5 ns	2.5 ns	0.0 ns
S60-1x	Not used	26.0 ns	0.0 ns + PR	19.0 ns	32.0 ns	13.0 ns	10.5 ns	4.5 ns
S60-1y	Not used	26.0 ns	3.0 ns + PR	11.0 ns	27.5 ns	12.5 ns	2.5 ns	0.0 ns

Figure 3: System configurations S60-1b, -1x, and -1y. The table indicates stands used (all dipoles EW-oriented) and the delays employed in each configuration. Note Stand 191 was accidentally phase reversed ("PR") due to a wiring error in the ARX interface, which affected only Configurations S60-1x and -1y.

6

Delay Line Units   Equal Lengths RG-58

ARX → DB64 →
ARX → DB64 →
ARX → DB64 →
ARX → DB64 →   Σ → ∇ → AAF → S60 → k1
ARX → DB64 →
ARX → DB64 →
ARX → DB64 →
ARX → DB64 →

Anti-aliasing Filters   FPGA Boards w/ Single-Channel Firmware   Linux PCs

ARX ──────────────→ AAF → S60 → k2

Configuration	187	189	191	210	212	214	228	230
S60-1c	38.5 ns	26.0 ns	3.0 ns	11.0 ns	27.5 ns	12.5 ns	2.5 ns	0.0 ns

Figure 4: System configuration S60-1c. The table indicates stands used (all dipoles EW-oriented) and the delays employed in each configuration. The stand associated with k2 is Stand 15.
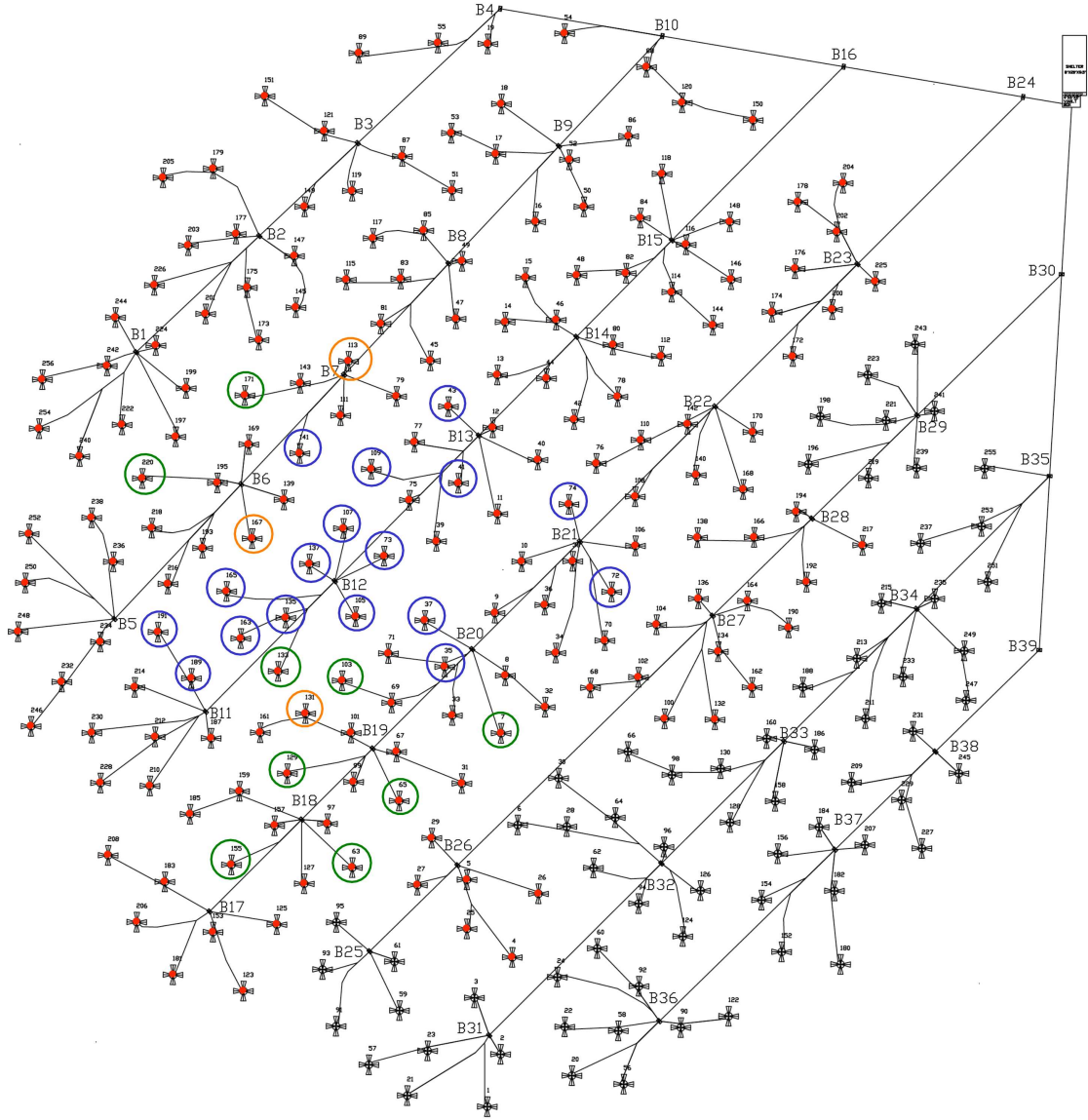
Figure 5: Stands used in the S60-2b and -2c beamformers. S60-2b used the stands indicated in blue and green only; S60-2c used all stands indicated in this figure.
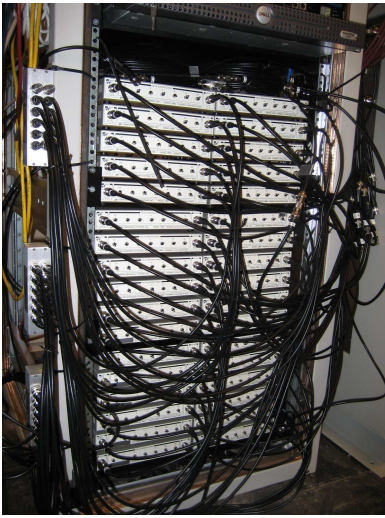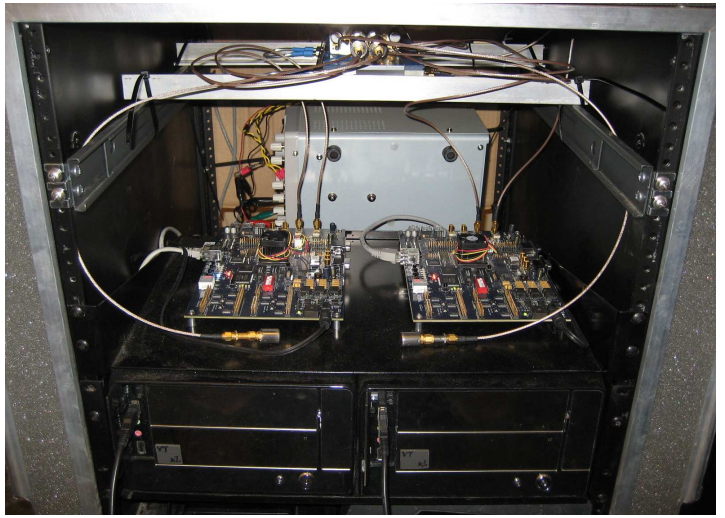
        (a) analog beamformer   (b) FPGA boards ("S60s") and PCs ("k1" & "k2")

Figure 6: Components of the S60-2 system. The 12-way power combiners are mounted along the left edge of the rack in (a). RF power splitters and anti-aliasing filters are partially visible on the top shelf in (b).
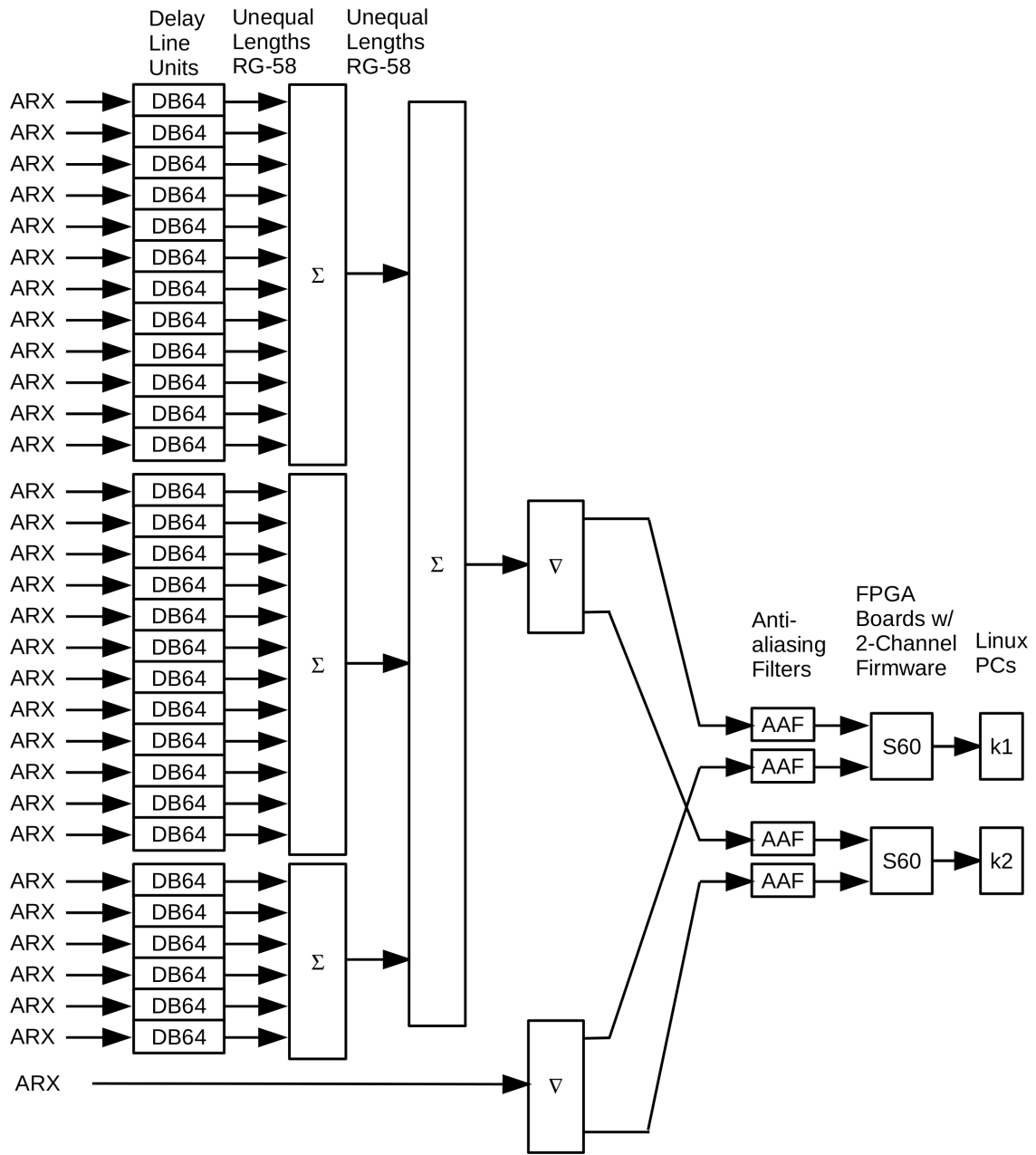
Figure 7: System configurations S60-2b, -2c, and -2d. The stand separate from the beamformer is always Stand 258.

```
 35 100   1.5
 37 100   0.0
 41 100  51.5
 43 100  63.5
 72 100  63.5
 73  50  34.0
 74 125  46.5
105  50  29.0
107  50  37.5
109 100  25.5
135  50  20.5
137  50  44.5
141  50  64.0
163   8  62.0
165  50   4.0
189   4  18.5
191   4   5.0
```

Table 1: S60-2b beamformer configuration table. The columns are stand ID, excess length of RG-58 used [ft], DB64 delay setting [ns]. This configuration may also be referred to as "B1" or "B1+" in other documentation.

```
     ---B2--- ---B3---
  7   50 45.0   50 44.0
 35  100  1.5  100  0.0
 37  100  0.0  100  0.0
 41  100 51.5  100 48.5
 43  100 63.5  100 62.5
 63    4  8.0    4  8.5
 65    4 61.5    4 61.5
 72  100 63.5  100 62.0
 73   50 34.0   50 31.0
 74  125 46.5  125 51.0
103   50 28.0   50 27.0
105   50 29.0   50 27.5
107   50 37.5   50 35.0
109  100 25.5  100 21.5
113             100 28.0  Not used in B2
129    4 53.5    4 53.0
131               4 64.5  Not used in B2
133    8 61.5    4 63.5
135   50 20.5   50 19.0
137   50 44.5   50 42.5
141   50 63.5   50 61.0
155    4  0.0    4  0.0
163    8 62.0    4 63.5
165   50  4.0   50  2.0
167              50  1.5  Not used in B2
171   54 62.0   50 63.5
189    4 18.5    4 17.5
191    4  5.0    4  3.0
220    4 63.5    4 63.5
```

Table 2: S60-2c beamformer configuration table. The columns are stand ID, excess length of RG-58 used [ft], DB64 delay setting [ns]. There are two versions of this configuration, identified as "B2" or "B3" in dataset documentation. The difference between these is number of dipoles used, and the exact values of the delays used: "B3" did not take into account antenna z coordinates, whereas "B4" did.

```
 35 100  7.0
 41 100 16.0
 43 100 14.0
 63   4 58.5
 65  50 26.5
 72 100 52.5
 73  50 14.5
 74 100 54.5
 89 100  9.5
103  50 37.0
105  50 24.0
107  50 12.5
109  50 63.5
113  50 47.0
129  50 12.5
131  29 44.0  Found low/no signal during teardown check.^2
133  14 60.0
135  50 16.0
137  50 27.5
141  50 23.0
155   4 50.5
163   8 62.5
165   4 63.5  Found low/no signal during teardown check.^2
167   4 52.5  Removed August 25, 2010 due to jabbering at ARX output.^1
171  50 14.5
189   4 28.0
191   4  4.0
195   4 60.0  Added July 29, 2010.  (Not present in first 2 datasets)
220   4 32.0
230   4  0.0  Found low/no signal during teardown check.^2
Footnotes:
^1  Last known good c. Jul 28.  Datasets between July 28 and Aug 25 may be affected.
^2  Unknown when these signals stopped working.  No jabbering noted.
```

Table 3: S60-2d beamformer configuration table. The columns are stand ID, excess length of RG-58 used [ft], DB64 delay setting [ns].
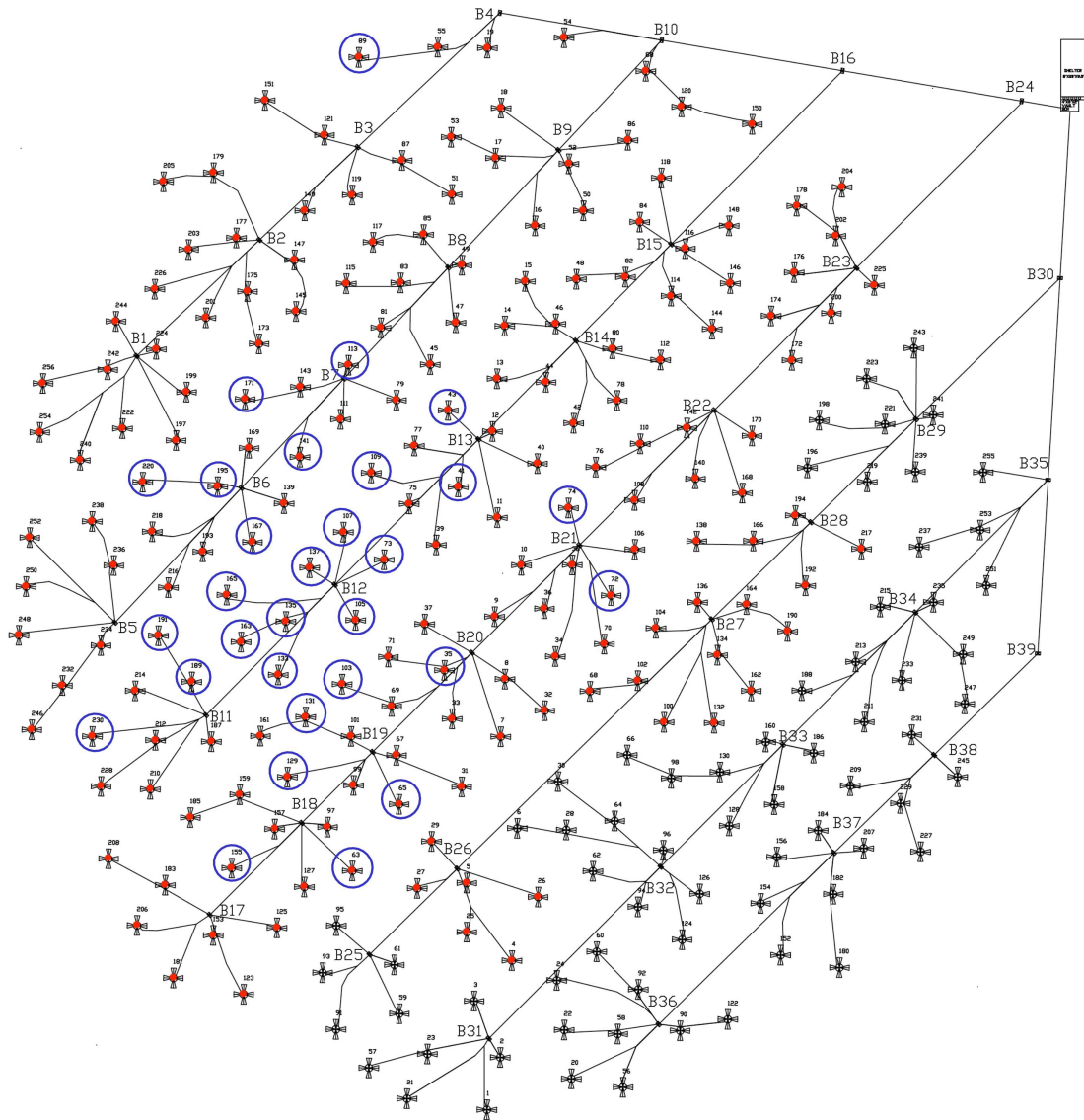
Figure 8: Stands used in the S60-2d beamformers. Stand 195 was not added until July 29, 2010. Stand 167 was removed on August 26.

3 Some Initial Results

In this section we show some initial "quick look" results from data acquired by the LWA1-S60 system. These results were generated while the system was in operation, and were intended to confirm reasonable performance from an engineering perspective. Additional analysis of data is presented in Sections 4.2 and 4.3, where it is used to validate model predictions of sensitivity and beam characteristics.

Figures 9 and 10 show a test observation using very short integrations from the S60-1a configuration that demonstrates the shape of the digital bandpass and gives an impression about the nature of radio frequency interference at the LWA-1 site. These results include the 38 MHz quasi-protected band (37.50–38.25 MHz) as well as spectrum above and below this band. Figure 10 shows the shape of the S60-1 version's band edges and relationship between adjacent channels.

Figure 11 shows spectral variance as a function of integration time from an experiment conducted using an 8-dipole beam from the S60-1 configuration. This result was obtained using the following procedure: A 4096-point FFT was applied, resulting in 915 Hz spectral channels. The outer 17% of the spectrum was discarded in order to obtain a relatively flat bandpass, and the remaining bandpass was calibrated (flattened) using a models of the ARX and S60 digital receiver frequency responses. The diurnal variation of system temperature, due to the changing sky brightness temperature distribution over time, was estimated from the data using a fit to 1 s total power measurements. Narrowband RFI was mitigated by blanking the 20% of spectral channels having the largest magnitudes,[4] reducing the effective bandwidth to 2.38 MHz. Note that the data appears to be noise-limited for integration times up to 1 h.

Figure 12 shows total power measurements taken over four consecutive days, "folded" onto a 1-day period to demonstrate the high level of daily repeatability that is achieved in the observations. This is a S60-1c observation (datasets 100414b_k1 and 100414b_k2), consisting of 2 s integrations sampled every 5 min simultaneously from a 8-dipole beam and a single dipole, both at a center frequency of 72.25 MHz. In this case no RFI mitigation is applied. The periodic behavior is due to the diurnal variation of system temperature resulting from the changing sky brightness temperature distribution over time. Note the difference between the single dipole and beam results; as expected the beam result exhibits more structure. In Section 4 we exploit this difference as a means to confirm beam shape and estimate sensitivity.

In the S60-2 configurations, the two outputs associated with each S60 are coherent, so it is technically possible to compute correlations between them. Unfortunately, the polarization of the "outrigger" stand (258) used as the second channel on each S60 is NS, whereas the polarization for the other channel is EW. Nevertheless, cross-polarized fringes from Cas A are strong enough to detect. Figure 13 shows Cas A-dominated fringes between Stands 230 and 258 (EW-oriented baseline of ≈ 300 m) obtained from the S60-1a datasets 100711_k1 and 100711_k2. An interesting finding from this result is the larger-than-expected difference between the fringe magnitudes between frequencies: With a spectral index of about -0.72 [8], Cas A at should be about 60% stronger at 38 MHz than at 74 MHz, whereas (as we shall see in Section 4) the system sensitivity is roughly equal at these two frequencies. Accounting for the difference in cable loss with frequency makes the predicted difference a factor of 3.2. However, Figure 13 shows the cross-polarized component of fringes is about 6.7 times stronger at 38 MHz than at 74 MHz. This seems to suggest the antenna cross-polarization is significantly better (i.e., lower) at 74 MHz than it is at 38 MHz. It will be interesting to see if this is borne out in LWA-1 commissioning observations.

---

[4]We now believe 20% blanking is excessively conservative for this dataset.
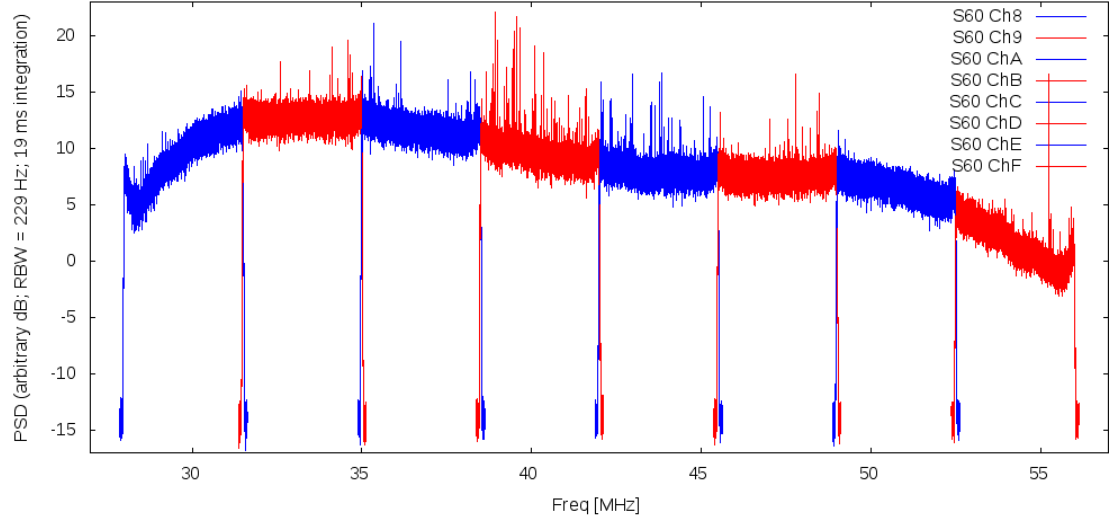
Figure 9: The spectrum appearing at the output of an ARX (thus, corresponding to a single dipole), created by acquiring one file at a time and tuning the FPGA board (S60-1 firmware) between acquisitions. The curved baseline is a combination of the Galactic noise spectrum variation and the not-quite-flat ARX bandpass. For this experiment, the ARX was configured for minimum bandwidth; almost all other datasets use the ARX in its *maximum* bandwidth configuration.
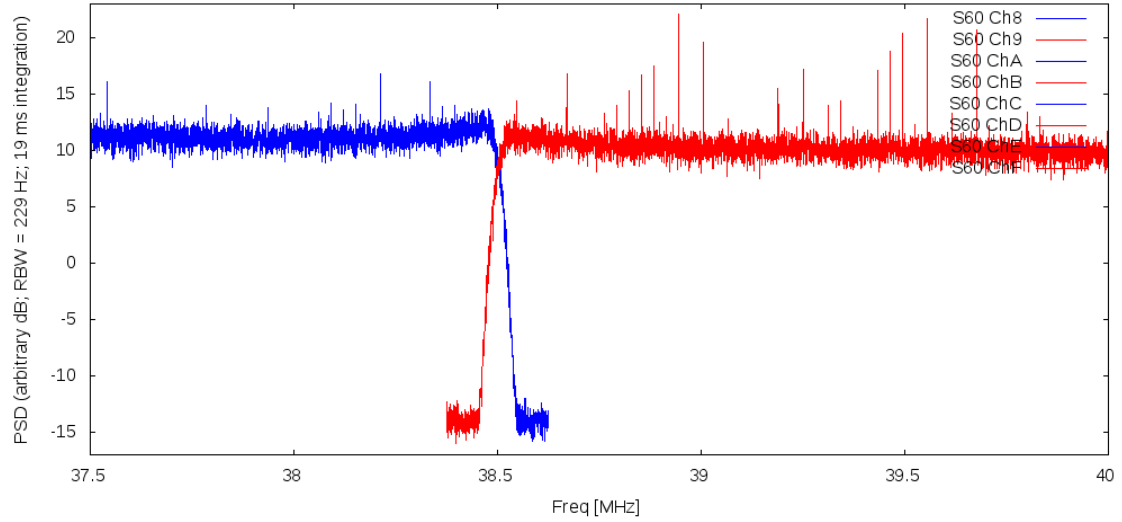
Figure 10: A close-up of Figure 9, including the 38 MHz radio astronomy band (37.50–38.25 MHz) and the crossover between adjacent S60-1 system tunings.

16
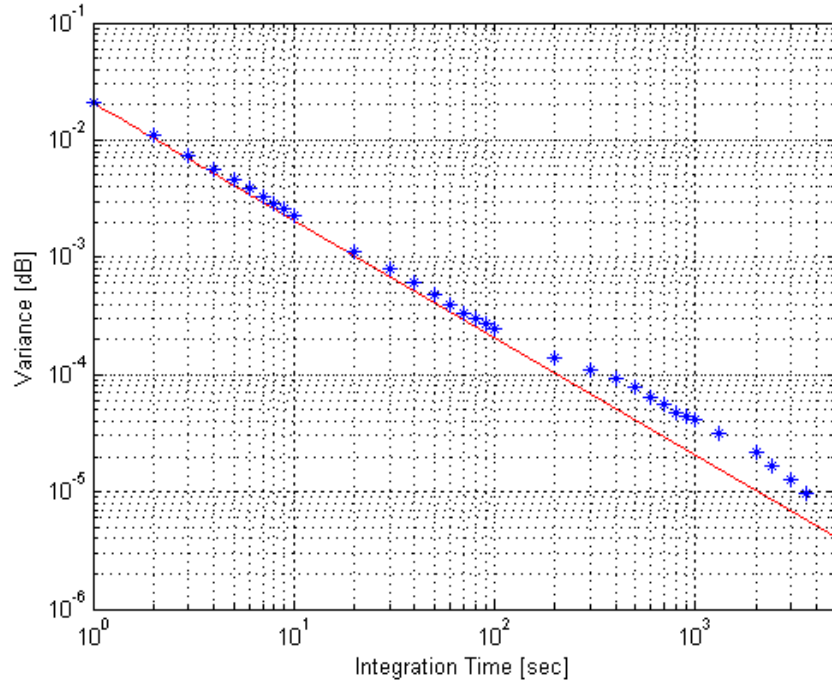
Figure 11: Demonstrating noise-limited sensitivity of the S60-1 system for integrations up to 1 h. 8-dipole beam, center frequency 72.25 MHz, effective bandwidth 2.38 MHz, 915 Hz spectral channels. From data collected between 02:00 and 03:00 local time. Frequency-domain blanking; see text for details.
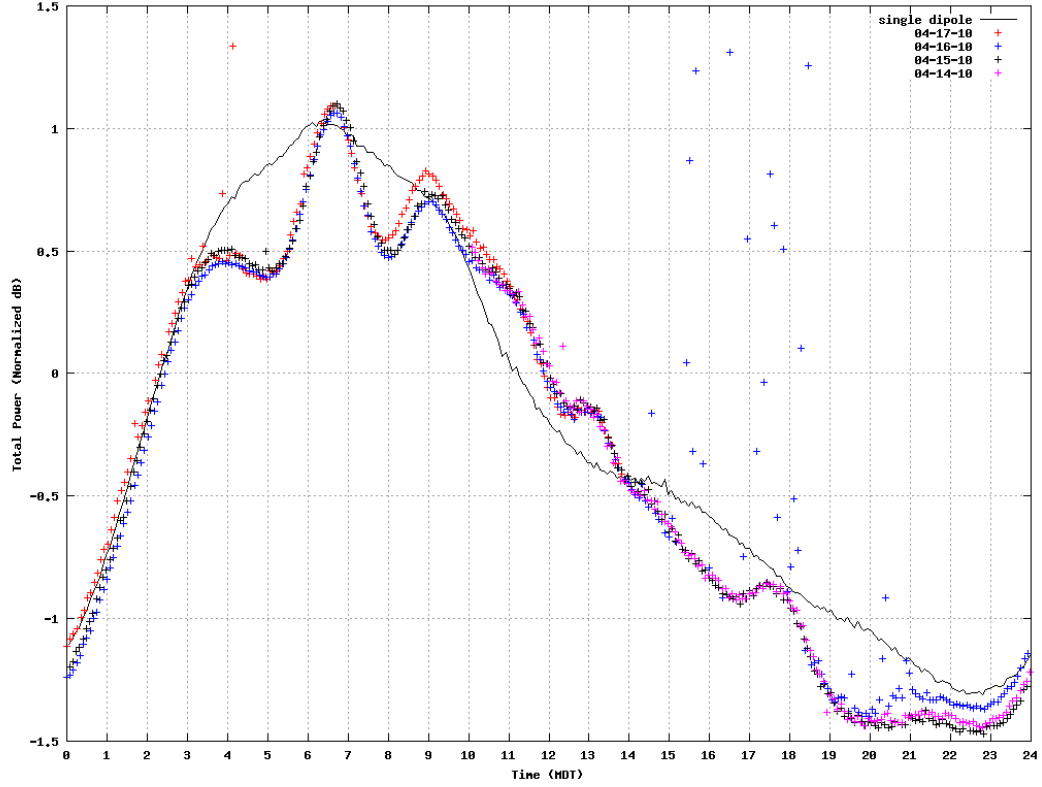
Figure 12: Total power measurements taken over four consecutive days and "folded" onto a 1-day period to demonstrate repeatability. Markers represent the beam data from each day, the solid line represents single-dipole data from one of these days. RFI between 1500 and 2100 on April 16 are believed to be due to thunderstorm activity.
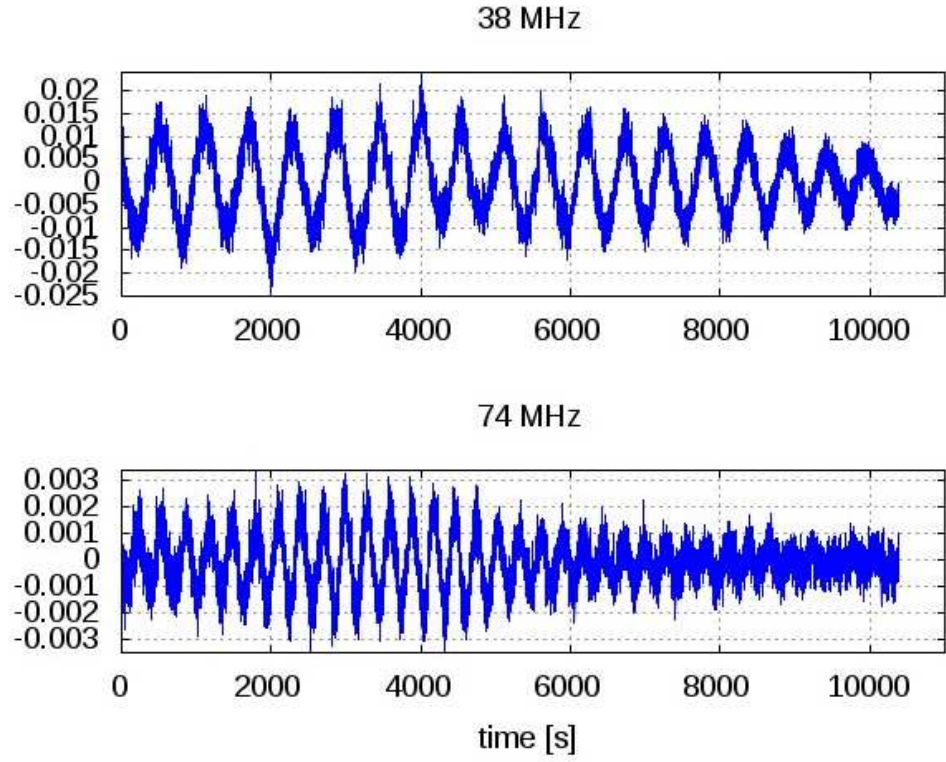
Figure 13: Real part of the correlation between Stands 230 (EW dipole) and 258 (NS dipole) around the time of Cas A upper culmination. The vertical scale is in arbitrary power units, but consistent between frequencies.

19

4 Characterization of System Performance

In this section we consider the performance of the LWA1-S60 system, in its various configurations, as an astronomical instrument. The two primary metrics of concern are *sensitivity* and *spatial selectivity*. These metrics are very difficult to determine directly by observation. Instead, we define in Section 4.1 a system model which can be used to estimate these metrics; then in Sections 4.2 and 4.3 we demonstrate that these estimates are consistent with acquired data.

4.1 System Model

We choose to characterize sensitivity in terms of *system equivalent flux density* (SEFD), defined for the purposes of this report to be the flux (Jy) of a discrete, spectrally-flat continuum source centered in the beam required to double the total power measured by the instrument. This can be determined as follows. The noise temperature associated with the source is

$$T = \frac{1}{2k} S \left[\epsilon A_e(\theta_0, \phi_0) \right] \ , \tag{1}$$

where $k = 1.38 \times 10^{-23}$ J/K, S is the source flux, $A_e(\theta_0, \phi_0)$ is effective aperture in the direction of the source, and ϵ is an efficiency factor that will be defined below. The noise temperature when the source is not present is defined as the *system temperature*, T_{sys}. For $S = $ SEFD, $T = T_{sys}$ and thus

$$\text{SEFD} = 2k \left(\frac{\epsilon A_e}{T_{sys}} \right)^{-1} \ . \tag{2}$$

The system temperature can be expressed as

$$T_{sys} = \epsilon T_A + T_R \ , \tag{3}$$

where T_A is the antenna temperature and T_R is the noise contribution from electronics following antennas. T_R is assumed to be 300 K, under the well-justified assumption that is dominated by the noise temperature of the FEE (see Section 2). T_A is defined in the usual manner as

$$T_A = \frac{1}{\Omega_A} \int_{sky} T_{sky}(\theta, \phi) \ p(\theta, \phi) \ \sin \theta d\theta d\phi \ , \tag{4}$$

where $p(\theta, \phi)$ is the normalized power pattern, $T_{sky}(\theta, \phi)$ is the sky brightness temperature distribution, and Ω_A is the *beam solid angle* defined as

$$\Omega_A = \int_{sky} p(\theta, \phi) \ \sin \theta d\theta d\phi \ . \tag{5}$$

The preceding definition of T_A presumes the antenna is perfectly lossless and perfectly-matched to the subsequent electronics. Since neither of these presumptions are true, ϵ is included to account for the efficiency of power transfer from antenna to electronics. The dominant factors in ϵ are *ground loss*, which is due to the electromagnetic coupling between antennas and the (lossy) ground, and *impedance mismatch efficiency* (IME), which accounts for the power reflected at antenna-electronics interface. IME has been estimated to be about 0.5 at both 38 MHz and 74 MHz for a standalone LWA-1 dipole (see Figure 2.5 of [9]), and roughly constant in between these frequencies. Ground loss efficiency is difficult to estimate, but is probably not worse than 0.5 at 38 MHz; see for example the analysis in [10].[5] On this basis, we presume $0.25 \leq \epsilon < 0.5$. We will see in Section 4.2 that

---

[5]Reference [10] indicates ground loss efficiency between -2.5 dB and -3.9 dB for frequencies between 30 MHz and 90 MHz for dipoles similar to those of LWA-1, but without ground screens. LWA-1 antennas use 3 m $\times$ 3 m ground screens, which will certainly improve ground loss efficiency, but since the ground screen is small relative to wavelength, the improvement is difficult to estimate. Thus, 0.5 seems like a reasonable estimate for the ground loss efficiency in this case.

$\epsilon = 0.25$ turns out to be consistent with observations.

It is important to note that ϵ must also be applied to A_e, as shown in Equations 1 and 2, since the same factors act to reduce the source power delivered from the antennas to the electronics. The effective aperture $A_e(\theta_0, \phi_0)$ is related to the directivity $D(\theta_0, \phi_0)$ as follows:

$$A_e(\theta_0, \phi_0) = \frac{\lambda^2}{4\pi} D(\theta_0, \phi_0) \qquad (6)$$

If we adopt the notation A_e and D (without indication of the θ and ϕ dependence) to mean the *maximum* values of these quantities, we have

$$D = \frac{4\pi}{\Omega_A} \qquad (7)$$

and thus

$$A_e = \frac{\lambda^2}{\Omega_A} \; . \qquad (8)$$

Then Equation 2 can be written conveniently as:

$$\text{SEFD} = 2k \left(\frac{\lambda^2/\Omega_A}{T_A + T_R/\epsilon} \right)^{-1} \qquad (9)$$

where the quantity inside the parentheses is $\epsilon A_e/T_{sys}$, and this is understood to be the sensitivity in the direction in which it is *maximum*; i.e., in the center of the beam, or at zenith when applied to an individual dipole.

4.2 Standalone Dipole

First we consider the performance of the NS-oriented dipole of Stand 258, which is located far from the station array and therefore is presumably not significantly affected by the presence of the other dipoles. Table 4 shows the results obtained following the theory of the previous section. The dipole power pattern is modeled using the method described in LWA Memo 175 [11]. The sky brightness temperature distribution $T_{sky}(\theta, \phi)$, which is required to compute T_{sys}, is obtained using the LWA MCS Sky Model (LMSM), described in LWA Engineering Memo MCS0037 [12]; which in turn is based on the "Global Sky Model" (GSM) of de Oliveira-Costa *et al.* (2008) [13]. Since T_A is a large fraction of the system temperature, T_{sys} varies diurnally as shown by example in Figures 14 and 15. The corresponding maximum and minimum values are shown in Table 4, from which the associated minimum and maximum SEFD is calculated using Equation 9. Also shown is the associated minimum detectable flux for 5σ confidence assuming the 1.86 MHz instantaneous bandwidth of the S60-2 system. It is interesting to note that the diurnal variation in T_A results in a roughly 2:1 variation, whereas there is hardly any difference at all in the sensitivity at 38 MHz versus 74.56 MHz.[6]

Rogers, Pratap, and Kratzenberg (2004) describe a method for calibrating low-frequency radio telescope arrays by comparing the observed diurnal variation in system temperature to that predicted using a system model combined with a model of sky brightness temperature [14]. We now use essentially the same idea to assess the performance of this S60-2 single-dipole configuration. Figures 14 and 15 show the results from a S60-2 observation conducted during the timeframe corresponding to the simulation results. The markers are total power in 1.86 MHz after 1.47 s integration, calculated every 5 minutes. The measured result is in arbitrary power units (i.e., not directly calibratible to absolute temperature units comparable to T_{sys}); instead the data is scaled by a constant determined so as to achieve the best fit to the bottom portion of the "Model (NS)" curve. The apparent interference observed daily during the afternoons is believed to due to regional thunderstorm activity. Despite this interference, note the excellent agreement between the "Model (NS)"

---

[6]The reason for this is that the λ^2 dependence of A_e approximately cancels the $\sim \lambda^{2.5}$ dependence of T_{sky}, which dominates T_{sys}.

(simulation) result and the observations calibrated in this manner. The agreement between theory and data also confirms our choice of $\epsilon = 0.25$ is reasonable, as it is found that significantly different values of ϵ result in worse agreement, regardless of the constant used to scale the observation data.

Finally, note that theory curves are plotted for EW-oriented dipole as well as the (actual) NS-oriented dipole. Interestingly, the NS result yields a significantly better fit to the data, suggesting that this type of measurement+analysis might be useful as a diagnostic to determine if dipole polarizations are wired correctly in the station array.

4.3 Configuration S60-2d Beamformer

We now consider the performance of the 30-dipole beamforming configuration (S60-2d, as defined in Section 2) that was in effect for the majority of the S60-2 observations. Table 5 shows the theory results, following the same procedure described in the previous section for the standalone dipole results. Once again, the dipole power patterns are modeled using the method described in LWA Memo 175; thus the effect of mutual coupling is being ignored. It is known that mutual coupling is expected to have only a very minor impact on the shape of the main lobe; also, the results of previous studies (see e.g., [1] and [15]) imply that effect of mutual coupling on sensitivity is degradation of not more than about 2 dB for high-elevation pointings not too close to the zenith.

The beam pattern is computed from the dipole pattern, taking into account cable delays (including dispersive delay) and losses, calculated using the models recommended in LWA Memo 170. This beamforming configuration also employs significant lengths of RG-58 coaxial cable as delay lines, and so these additional delays and losses are also taken into account.[7] The resulting normalized power patterns ($p(\theta, \phi)$ in the terminology of Section 4.1) are shown in Figures 16 and 17. Beam size, peak sidelobe level, and main lobe efficiency (Ω_B/Ω_A) are summarized in Table 5. It should be noted that the 38 MHz beam has high sidelobes, but is otherwise not too bad. The 74.56 MHz beam, on the other hand, is relatively crummy, with a main lobe efficiency of only about 10% and very high sidelobes. This is due the large (1.25λ minimum, typically larger) Nyquist-deficient spacings between stands in combination with the small (relative to the full 256-stand station array) number of stands used in this configuration. Interestingly, this does not significantly degrade the sensitivity, which (as is noted below) is still improved over the single-dipole system by a factor roughly equal to the number of dipoles. As a spatial filter, however, the 74.56 MHz beam is very poor, and the 38 MHz beam is not great.

Following the same procedure described in Section 4.2, Figures 18 and 19 show the theory results as well as the observation data corresponding to the simulation. Note that the observation and model results show good agreement, although with a few exceptions. The large difference in the 38 MHz result around 23:00 local time (LT) (and occurring at the same time the next day) is difficult to explain. Our best guess is that this due to a strong source moving through a sidelobe, which might explain the difference since we expect the actual sidelobes to be significantly different from the model sidelobes due to mutual coupling. On the bright side,[8] it is encouraging to see a peak just before 10:00 LT corresponding to the passing of Tau A through the center of the beam. Using the same procedure as Hartman (2009) [16], we estimate the flux of Tau A to be roughly 2170 Jy and 1810 Jy at 38 MHz and 74 MHz respectively, yielding an expected signal-to-noise ratio of about 13 (about the same at both frequencies) with respect to the bandwidth and integration times used here.

Finally, we should emphasize that the results shown in this section apply specifically to the S60-1d beamformer configuration. The same analysis is straightforward to apply to the other S60-1 and S60-2 beamforming configurations, but of course the results will be significantly different.

---

[7]In the terminology of LWA Memo 170, we model RG-58 as having velocity factor 0.66, dispersive delay 4.78 ns per 100 m at 10 MHz, and $\alpha_0 = 0.00535$ m^{-1} at $f_0 = 10$ MHz.

[8]Please excuse the pun.

Freq.	FWHM E-Plane/H-Plane	Ω_A	T_{sys}	SEFD	S_{min}[1]	S_{min}[2]
38 MHz	90°/110°	2.35 sr	4100 K	1706.7 kJy	6257 Jy	617 Jy
			2250 K	936.6 kJy	3434 Jy	338 Jy
74.56 MHz	80°/116°	2.42 sr	1100 K	1815.3 kJy	6655 Jy	656 Jy
			700 K	1155.2 kJy	4235 Jy	417 Jy

[1] Minimum detectable flux at 5σ confidence for 1.86 MHz bandwidth and 1 s integration.
[2] Minimum detectable flux at 5σ confidence for 1.86 MHz bandwidth and 103 s integration.

Table 4: Estimate of S60-2 performance in configurations using a single standalone NS-oriented dipole.

Freq.	FWHM Az/Alt	Peak Sidelobe	Ω_B/Ω_A	Ω_A	T_{sys}	SEFD	S_{min}[1]	S_{min}[2]
38 MHz	65°/12°	−10 dB	∼ 0.4	0.0775 sr	4000 K	54.9 kJy	201 Jy	20 Jy
					2000 K	27.5 kJy	101 Jy	10 Jy
74.56 MHz	35°/7°	−6 dB	∼ 0.1	0.0841 sr	1050 K	60.4 kJy	221 Jy	22 Jy
					650 K	37.3 kJy	137 Jy	13 Jy

[1] Minimum detectable flux at 5σ confidence for 1.86 MHz and 1 s.
[2] Minimum detectable flux at 5σ confidence for 1.86 MHz and 103 s.

Table 5: Estimate of S60-2d performance (30 EW-oriented dipoles).
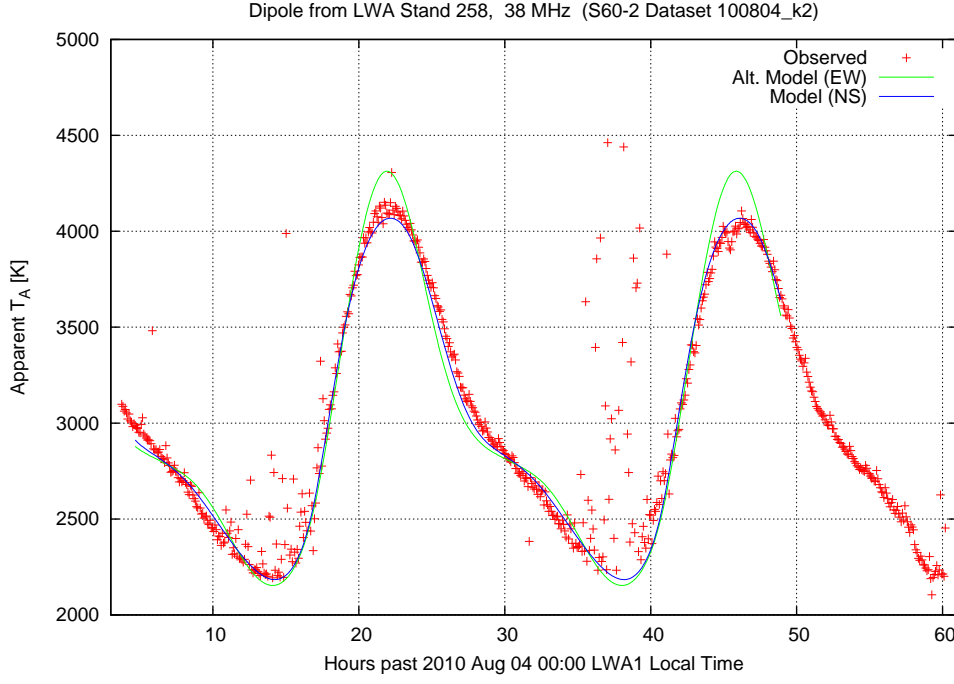
Figure 14: System temperature for Stand 258 as a standalone dipole at 38 MHz. Note "Apparent T_A" is equivalent to T_{sys} as defined in Equation 3. The solid lines are theory results, with "Model (NS)" corresponding to the NS-oriented dipole, and "Alt Model (EW)" corresponding to the EW-oriented dipole. The markers are the observed results (i.e., from captured data) for the NS-oriented dipole.

Figure 15: System temperature for Stand 258 as a standalone dipole at 74.56 MHz. See caption of Figure 14 for additional explanation.
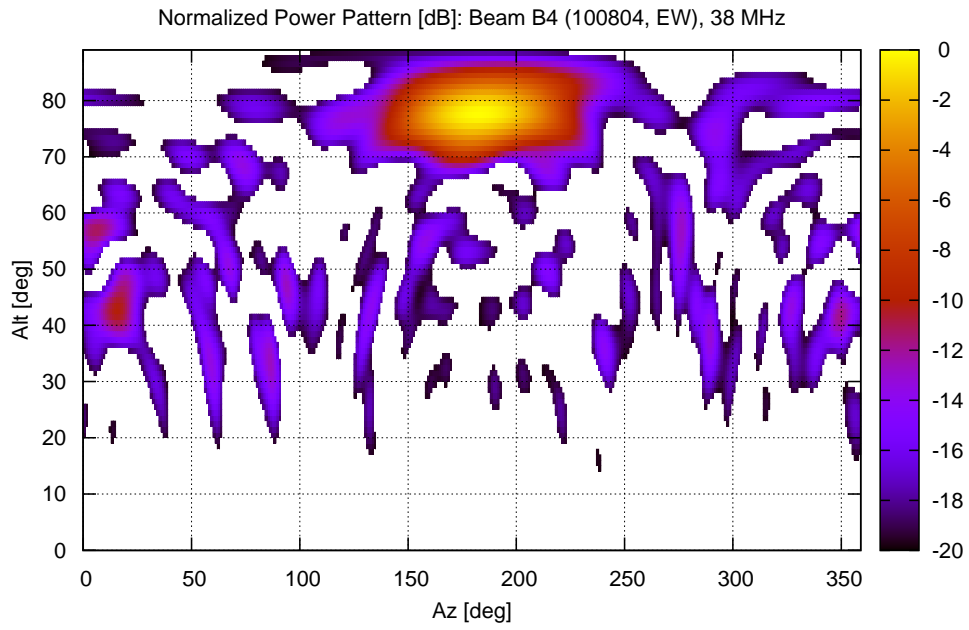
Figure 16: Normalized power pattern of the S60-2d configuration beam at 38 MHz. Values below −20 dB are not plotted.
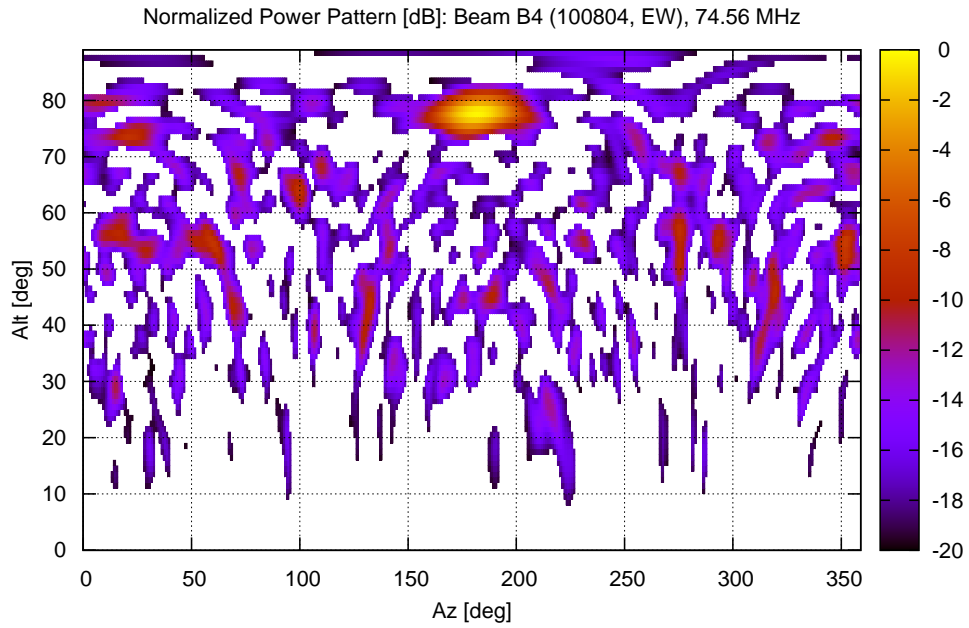
Figure 17: Normalized power pattern of the S60-2d configuration beam at 74.56 MHz. Values below −20 dB are not plotted.
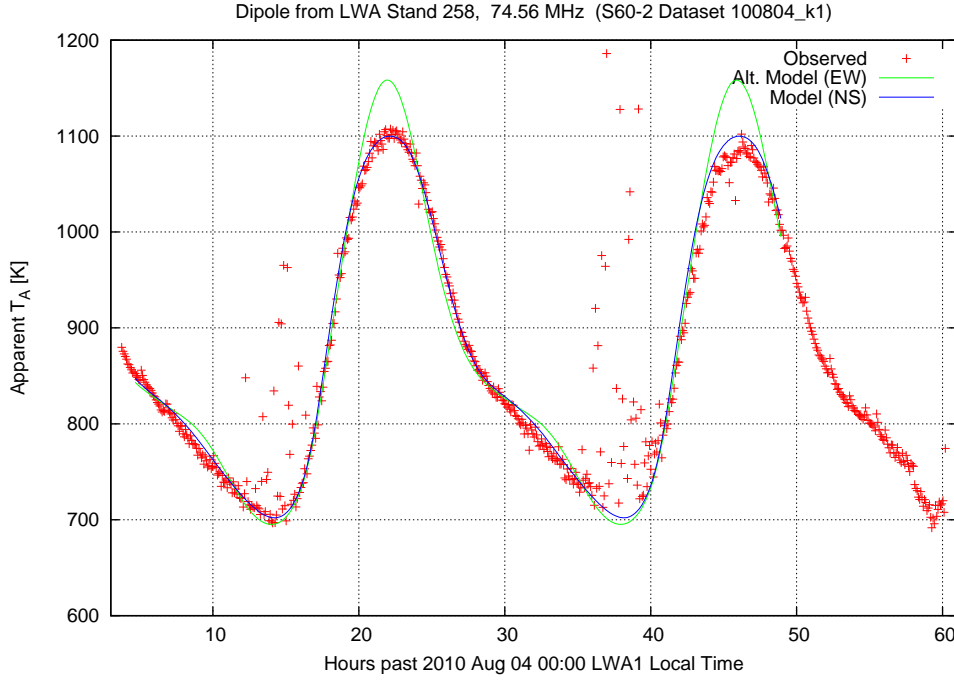
25
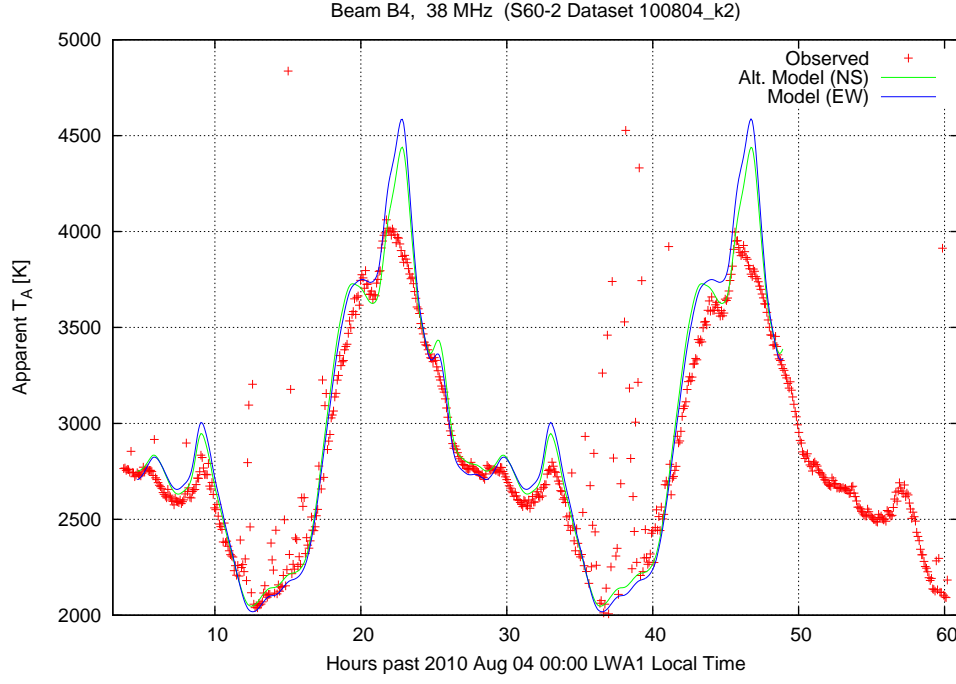
Figure 18: System temperature for the S60-2d beam (30 EW-oriented dipoles pointing South at a zenith angle of 12°) at 38 MHz. Note "Apparent T_A" is equivalent to T_{sys} as defined in Equation 3. The solid lines are simulation results, with "Model (EW)" corresponding to the actual beam, and "Alt Model (NS)" corresponding to the predicted result if the beam were comprised of NS-oriented (as opposed to EW-oriented) dipoles. The markers are observed results for the actual (EW-oriented dipole) array.
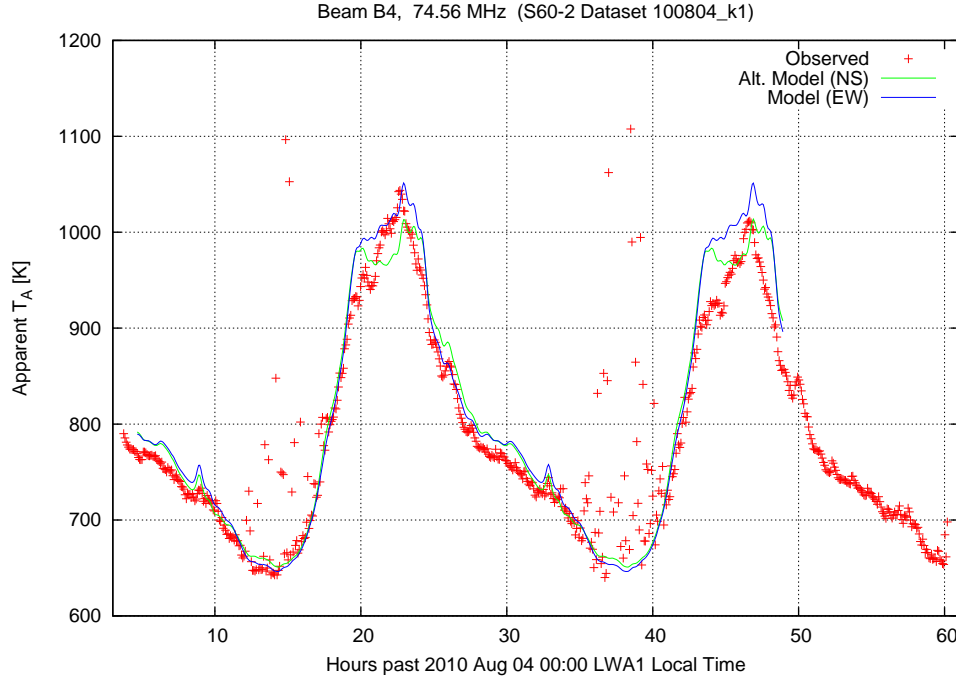
Figure 19: System temperature for the S60-2d beam (30 EW-oriented dipoles pointing South at a zenith angle of 12°) at 74.56 MHz. See caption of Figure 18 for additional explanation.

A Acknowledgments

B   Document History

- Version 2 (Dec 21, 2010):
  - Noted that Stands 131, 165, and 230 were "no sig" upon teardown of the S60-2d configuration.
  - Very minor revisions to estimates of SEFD and S_{min} in tables.
- Version 1 (December 12, 2010): First version.

C Observations

A summary of available data appears in Table 6. A detailed listing begins on the next page. See end of listing for explanatory notes.

Configuration	Data Size	"Low Duty Cycle" Observing	Continuous (100% Duty Cycle) Observing
S60-1a	60.9 GB	31 h	2.2 h
S60-1b	1154.3 GB	107 h	27.3 h
S60-1c	1771.9 GB	152 h	35.1 h
S60-1x	1729.2 GB	10 h	35.8 h
S60-1y	3883.0 GB	50 h	93.6 h
TOTAL, S60-1	**8.4 TB**	**350 h**	**194.0 h**
S60-2a	57.4 GB	0	8.6 h
S60-2b	197.8 GB	20 h	2.9 h
S60-2c	1439.9 GB	13 h	22.9 h
S60-2d	7072.7 GB	123 h	137.3 h
TOTAL, S60-2	**9.1 TB**	**156 h**	**171.7 h**
TOTAL, All Configurations	**17.5 TB**	**506 h**	**365.7 h**

Table 6: A summary of data collected in the various configurations of the LWA-S60 system.

```
Summary of data collected using the LWA1-S60 System
Steve Ellingson
December 11, 2010


   Start   Start         k1    k2
   Date    Time  Src Src Freq  Freq
d YYMMDD   HHMM   A   B  [MHz]  [MHz]  (A)  (B)    (C)    dataset    MB     Intended or possible use; other remarks
-- ------  ----  --- --- ----- ----- ----- --- ------- ---------- ------- ----------------------------------------


=== The following datasets are taken in the S60-1a configuration ============================================
 1 100108  unkn  112 --- var.  ----- var.  --- -------            2200  Scanning through S60 tunings
 1 100108  1600  112 --- 36.75 ----- 0.2 s  15     16 h  100108o_*    91  Diurnal variation
 1 100109  unkn  112 --- 36.75 ----- 60 s   ~0     16 s  100109a    6600  Deep integration
 1 100109  1712  214 --- 36.75 50.75 0.2 s  15     15 h  100109o_*   168  Diurnal variation
 1 100110  unkn  ^1  ---  1.75 ----- 60 s   --- ------- 100110b_k1   420  Diagnostic/calibration
 1 100110  unkn  ^1  --- ----- 1.75  60 s   --- ------- 100110b_k2   420  Diagnostic/calibration
 1 110110  unkn  ^2  ---  1.75 ----- 60 s   --- ------- 100110b_k1   420  Diagnostic/calibration
 1 110110  unkn  214 --- 36.75 ----- 60 s   --- ------- 100110b_k1   420  Diagnostic/calibration
 1 110110  unkn  191 --- 36.75 ----- 60 s   --- ------- 100110b_k1   420  Diagnostic/calibration
 1 110110  unkn  228 --- 36.75 ----- 60 s   --- ------- 100110b_k1   420  Diagnostic/calibration
 1 110110  unkn  189 --- 36.75 ----- 60 s   --- ------- 100110b_k1   420  Diagnostic/calibration
 1 110110  1230  214 --- 36.75 ----- 60 s   ~0     66 m  100110c_k1 25200  Deep integration, RFI
 1 110110  1230  214 --- ----- 33.25 60 s   ~0     66 m  100110c_k2 25200  Deep integration, RFI
Footnotes:
^1  1.775 MHz sine, 4 Vpp applied at reference point [G]
^2  DS345 noise, 4 Vpp applied at reference point [G]

=== The following datasets are taken in the S60-1x configuration (beam is 7 dipoles pointing Z=36 deg to S) ^3 ====
 1 100111  2100  BF  --- 36.75 33.25 140 s  ~0    3.9 h  100111a_*  191499  CGP (at ~3dB point in beam) ^4
 1 100112  0200  BF  --- 36.75 33.25 140 s  ~0    3.9 h  100111b_*  191499  B0950+08 transits through center ^4
Footnotes:
^3  Stand 191 was phase-reversed in this configuration
^4  Time offset between k1 and k2 PCs was up to 2 minutes in these datasets.  See field notes for details.

=== The following datasets are taken in the S60-1y configuration (beam is 7 dipoles pointing Z=22 deg to S) ^3 =====
 1 100112  2100  BF  --- 36.75 33.25 140 s  ~0    3.9 h  100112a_*  191499  CGP transits through center ^4
 1 100113  2100  BF  --- 36.75 33.25 140 s  ~0    3.9 h  100113_*   191499  CGP transits through center ^4
 1 100116  0630  BF  --- 36.75 50.75   2 s  15     24 h  100116_*     2819  Diurnal variation ^4
 2 100117  2200  BF  --- 36.75 50.75 140 s  ~0    3.9 h  100117_*   191499  CGP transit 2200 ^4
```

```
 2 100118  2100  BF  --- 36.75 50.75 140 s  ~0    3.9 h 100118_*    191499  CGP transits through center ^4
 2 100120  0100  BF  --- 36.75 50.75 140 s  ~0    3.9 h 100120_*    191499  SDP, Deep int.; k2's S60 stopped early ^4
 2 100122  2100  BF  --- 36.75 ----- 140 s  ~0    3.9 h 100122_k1    98000  CGP transits through center
 2 100124  1255  BF  --- 36.75 ----- 280 s  ~0   14 min 100124d_k1    5880  Daylight RFI, deep integration
 2 100124  2100  BF  --- 36.75 ----- 280 s  ~0    3.9 h 100124_k1    98000  CGP transits through center
 2 100125  0900  BF  --- 36.75 ----- 280 s  ~0    3.9 h 100125a_k1   98000  Daylight RFI, deep integration, SDP
 2 100125  1930  BF  --- 36.75 -----   2 s  15    23 h 100125b_k1    1302  Diurnal variation
 2 100127  0535  BF  --- 36.75 -----   2 s  15   2.5 h 100127a_k1     140  Diurnal variation
Footnotes:
^3  Stand 191 was phase-reversed in this configuration
^4  Time offset between k1 and k2 PCs was up to 2 minutes in these datasets.  See field notes for details.


=== The following datasets are taken in the S60-1x configuration (beam is 7 dipoles pointing Z=36 deg to S) ^3 ====
 2 100127  1020  BF  --- 36.75 50.75   2 s  15    10 h 100127b_*     3892  Diurnal variation. k1 starts before k2
 2 100128  0030  BF  --- 36.75 50.75 280 s  ~0    3.9 h 100128a_*   188160  B0950+08 @ 0130. k1 starts late
 2 100128  0600  BF  --- 36.75 50.75 280 s  ~0    3.9 h 100128b_*   196000  SDP, early morning RFI survey
 2 100128  1130  BF  --- 36.75 50.75 280 s  ~0    3.9 h 100128c_*   196000  Transits: Jupiter 1400 (48deg)
 2 100128  1700  BF  --- 36.75 50.75 280 s  ~0    3.9 h 100128d_*   196000  SDP, early evening RFI survey
 3 100128  2330  BF  --- 36.75 50.75 280 s  ~0    3.9 h 100128e_*   196000  B0950+08 transit 0130; SDP
 3 100129  0445  BF  --- 36.75 50.75 280 s  ~0    3.9 h 100129a_*   196000  SDP, early morning RFI survey
 3 100129  1130  BF  --- 36.75 50.75 280 s  ~0    3.9 h 100129b_*   196000  Transits: Jupiter; SDP. k1 stopped early
 3 100129  2330  BF  --- ----- 50.75 280 s  ~0   46 min 100129c_k2   19600  B0950+08 transit 0130; SDP
Footnotes:
^3  Stand 191 was phase-reversed in this configuration


=== The following datasets are taken in the S60-1y configuration (beam is 7 dipoles pointing Z=22 deg to S) ^3 =====
 3 100203  1945  BF  --- 36.75 50.75 280 s  ~0    3.9 h 100203a_*   131320  Crab transit 2045. k2 stopped early. ^5
 3 100204  1941  BF  --- 36.75 ----- 140 s  ~0    3.9 h 100204a_k1   98000  Crab transit 2041
 3 100205  1937  BF  --- 36.75 ----- 140 s  ~0    3.9 h 100205a_k1   98000  Crab transit 2037
 3 100211  1917  BF  --- 36.75 50.75 140 s  ~0    3.9 h 100211_*    196000  Crab transit 2017
 3 100212  1913  BF  --- 36.75 50.75 140 s  ~0    3.9 h 100212_*    196000  Crab transit 2013
 3 100213  1909  BF  --- 36.75 50.75 140 s  ~0    3.9 h 100213_*    196000  Crab transit 2009
 3 100214  1905  BF  --- 36.75 50.75 140 s  ~0    3.9 h 100214_*    196000  Crab transit 2005
 4 100215  1901  BF  --- 36.75 50.75 140 s  ~0    3.9 h 100215_*    133280  Crab transit 2001. k1 stopped early.
 4 100217  0100  BF  --- ----- 50.75 140 s  ~0    3.9 h 100217_k2    98000  SDP, deep integration
 4 100218  0100  BF  --- 36.75 50.75 140 s  ~0    3.9 h 100218_*    196000  SDP, deep integration
 4 100219  0100  BF  --- 36.75 50.75 140 s  ~0    3.9 h 100219_*    196000  SDP, deep integration
 4 100220  0100  BF  --- 36.75 50.75 140 s  ~0    3.9 h 100220_*    196000  SDP, deep integration
 4 100220  1834  BF  --- 36.75 50.75 140 s  ~0    3.9 h 100220a_*   196000  Crab transit 1934
```

```
4 100221  1800  BF  --- 36.75 50.75 140 s  ~0   3.9 h 100221_*    196000  Crab transit 1930
4 100223  0100  BF  --- 36.75 50.75 140 s  ~0   3.9 h 100223_*    196000  SDP, deep integration
4 100224  0100  BF  --- 36.75 50.75 140 s  ~0   3.9 h 100224_*    196000  SDP, deep integration
Footnotes:
^3  Stand 191 was phase-reversed in this configuration
^5  Filename timestamps read "2009" (as opposed to "2010") in this dataset.

=== The following datasets are taken in the S60-1b configuration (beam is 8 dipoles pointing Z=23 deg to S) ========
4 100324  1600  BF  --- 72.75 22.75 140 s  ~0   3.9 h 100324_k*  196000  CGP @1732. NOTE: k2 data on drive "5" ^8
5 100325  0001  BF  --- 72.75 22.75 140 s  ~0   3.9 h 100325a_*  196000  SDP, nightime deep integration. ^8
5 100325  0600  BF  --- 72.75 22.75 140 s  ~0   3.9 h 100325b_k* 196000  Daytime RFI, deep integration. ^8
5 100325  1530  BF  --- 72.75 22.75 140 s  ~0   3.9 h 100325c_*  196000  CGP transit 1728 ^8
5 100326  0001  BF  --- 72.75 22.75 140 s  ~0   3.9 h 100326a_k* 196000  SDP, nightime deep integration ^8
5 100326  1400  BF  --- 72.75 22.75   2 s  15    17 h 100326b_k*    966  Diurnal variation ^8
5 100327  1400  BF  --- ----- 22.75   2 s  15    66 h 100327b_k2   3682  Diurnal variation ^8
5 100327  1600  BF  --- 72.75 ----- 140 s  ~0   3.9 h 100327a_k1  98000  CGP transit 1720 ^8
5 100328  1600  BF  --- 72.75 ----- 140 s  ~0   3.9 h 100328_k1   98000  CGP transit 1716 ^8
5 100329  0935  BF  --- 72.75 -----   2 s  15    24 h 100329_k1    1372  Diurnal variation ^8
Footnotes:
^8  In these datasets, the 72.75 MHz signal should be checked for evidence of gain compression or intermod.

=== The following datasets are taken in the S60-1c configuration (beam is 8 dipoles pointing Z=23 deg to S) ========
5 100413  1500  BF   15 72.75 72.75 140 s  ~0   3.9 h 100413a_k*  196000  CGP transit 1621 ^7
6 100414  0100  BF   15 72.75 72.75 140 s  ~0   3.9 h 100414a_k*  196000  SDP, nightime deep integration ^7
6 100414  1005  BF   15 72.75 72.75   2 s   5    76 h 100414b_k*   25200  Diurnal var. k2 starts 25 m late ^7
5 100419  1430  BF   15 72.75 72.75 140 s  ~0   3.9 h 100419a_k*  196000  CGP transit 1557 ^7
6 100420  1430  BF   15 72.75 72.75 140 s  ~0   3.9 h 100420a_k*  196000  CGP transit 1553 ^7
6 100421  0100  BF   15 72.75 72.75 140 s  ~0   3.9 h 100421a_k*  196000  SDP, nightime deep integration ^7
5 100421  1430  BF   15 72.75 72.75 140 s  ~0   3.9 h 100421b_k*  196000  CGP transit 1549 ^7
6 100422  1430  BF   15 72.75 72.75 140 s  ~0   3.9 h 100422a_k*  196000  CGP transit 1545 ^7
7 100507  0700  BF   15 72.75 72.75   2 s   5    76 h 100507_k*    25200  Diurnal variation
7 100511  1300  BF   15 72.75 72.75 140 s  ~0   3.9 h 100511a_k*  196000  CGP transit 1416
7 100512  0100  BF   15 72.75 72.75 140 s  ~0   3.9 h 100512_k*   196000  Overnight SDP, deep integration
Footnotes:
^7  In these datasets, the anti-aliasing filter used for the k2/Stand15 signal is about 2~MHz wide; that is,
    narrower than the digital bandpass.

=== The following datasets are taken in the S60-2a configuration ===================================================
7 100711  0300  230 258 74.56 38.00 103 s  ~0   2.86 h 100711_k*  196000  Cas A high-alt transit
```

```
  7 100712  0030  230 258 74.56 38.00 103 s  ~0    2.86 h 100712a_k* 196000  Cyg A high-alt transit

=== The following datasets are taken in the S60-2b configuration (beam is 17 dipoles pointing Z=24.8 deg to N) =====
  7 100713  0350  B1  258 74.56 38.00 103 s  ~0    2.86 h 100713a_k* 196000  Cas A high-alt transit
  7 100713  1150  B1+ 258 74.56 38.00 1.47 s  5   19.68 h 100713b_k*   6594  Diurnal variation

=== The following datasets are taken in the S60-2c configuration (beam is 26 or 30 dipoles pointing Z=24.8 deg to N)
  7 100715  0350  B2  258 74.56 38.00 103 s  ~0    2.86 h 100715a_k2  98000  Cas A high-alt transit
  7 100715  1800  B3  258 74.56 38.00 1.47 s  5   13.45 h 100715b_k*   4508  Diurnal variation

=== The following datasets is taken in the S60-2a configuration =====================================================
  7 100716  0942  230 258 74.56 38.00 103 s  ~0    2.86 h 100716a_k* 196000  Tau A high-alt transit

=== The following datasets are taken in the S60-2c configuration (beam is 26 or 30 dipoles pointing Z=24.8 deg to N)
  6 100717  0330  B3  258 74.56 38.00 103 s  ~0    2.86 h 100717a_k* 196000  Cas A high-alt transit
  6 100718  0038  B3  258 74.56 38.00 103 s  ~0    2.86 h 100718b_k* 196000  Same as 100717a_k*, but earlier.
  6 100718  2146  B3  258 74.56 38.00 103 s  ~0    2.86 h 100718c_k* 196000  Same as 100717a_k*, but earlier.
  6 100719  1854  B3  258 74.56 38.00 103 s  ~0    2.86 h 100719a_k* 196000  Same as 100717a_k*, but earlier.
  7 100720  1603  B3  258 74.56 38.00 103 s  ~0    2.86 h 100720_k*  196000  Same as 100717a_k*, but earlier.
  7 100721  0914  B3  258 74.56 38.00 103 s  ~0    2.86 h 100721a_k* 196000  Same as 100717a_k*, but later.
  8 100722  0621  B3  258 74.56 38.00 103 s  ~0    2.86 h 100722a_k* 196000  Same as 100717a_k*, but later.

=== The following datasets are taken in the S60-2d configuration (beam is 30+/- dipoles pointing Z=12 deg to N) ====
  8 100722  2326  B4  258 74.56 38.00 103 s  ~0    2.86 h 100722b_k* 196000  B1919+21 transit.
  8 100723  0944  B4  258 ----- 38.00 103 s  ~0    2.86 h 100723a_k1  98000  Tau A / CGP transit
  8 100802  2214  B4  258 74.56 38.00 103 s  ~0    2.86 h 100802a_k* 196000  B1919+21 transit ^6
  8 100803  0831  B4  258 74.56 38.00 103 s  ~0    2.86 h 100803a_k* 196000  Tau A / CGP transit ^6
  8 100804  0440  B4  258 74.56 38.00 1.47 s  5    ~58 h 100804_k*   19362  Diurnal variation ^6
  8 100807  0815  B4  258 74.56 38.00 103 s  ~0    2.86 h 100807_k*  196000  Tau A / CGP transit ^6
  8 100817  0736  B4  258 74.56 38.00 103 s  ~0    2.86 h 100817_k*  196000  Tau A / CGP transit ^6
  8 100822  0716  B4  258 74.56 ----- 103 s  ~0    2.86 h 100822_k1   98000  Tau A / CGP transit ^6
  8 100822  1300  B4  258 74.56 ----- 1.47 s  5    ~65 h 100822b_k1  10906  Diurnal variation ^6
  8 100826  0100  B4  258 74.56 38.00 103 s  ~0    2.86 h 100826a_k* 196000  Overnight SDP
  9 100826  2041  B4  258 74.56 38.00 103 s  ~0    2.86 h 100826b_k* 196000  B1919+21 transit
  9 100828  0052  B4  258 74.56 38.00 103 s  ~0    2.86 h 100828a_k* 196000  Overnight SDP
  9 100829  0658  B4  258 74.56 38.00 103 s  ~0    2.86 h 100829_k*  140140  Tau A / CGP transit. k1 froze after 43%
  8 100830  0044  B4  258 ----- 38.00 103 s  ~0    2.86 h 100830_k2   98000  Overnight SDP
  9 100831  0040  B4  258 ----- 38.00 103 s  ~0    2.86 h 100831_k2   98000  Overnight SDP
  9 100901  0036  B4  258 ----- 38.00 103 s  ~0    2.86 h 100901_k2   98000  Overnight SDP
```

```
 9 100901  0646  B4  258 ----- 38.00 103 s  ~0    2.86 h 100901a_k2  98000   Tau A / CGP transit
 9 100902  0032  B4  258 ----- 38.00 103 s  ~0    2.86 h 100902a_k2  98000   Overnight SDP
 9 100903  0028  B4  258 ----- 38.00 103 s  ~0    2.86 h 100903a_k2  98000   Overnight SDP
 9 100903  0638  B4  258 ----- 38.00 103 s  ~0    2.86 h 100903b_k2  98000   Tau A / CGP transit
 9 100904  0604  B4  258 ----- 38.00 103 s  ~0    2.86 h 100904a_k2  98000   Tau A / CGP transit (Sat AM)
 9 100905  0630  B4  258 ----- 38.00 103 s  ~0    2.86 h 100905_k2   98000   Tau A / CGP transit (Sun AM)
 9 100907  0012  B4  258 ----- 38.00 103 s  ~0    2.86 h 100907a_k2  98000   Overnight SDP
 9 100908  0008  B4  258 ----- 38.00 103 s  ~0    2.86 h 100908a_k2  98000   Overnight SDP
 9 100909  0004  B4  258 ----- 38.00 103 s  ~0    2.86 h 100909a_k2  98000   Overnight SDP
 9 100909  2359  B4  258 ----- 38.00 103 s  ~0    2.86 h 100909b_k2  98000   Overnight SDP
10 100911  0610  B4  258 ----- 38.00 103 s  ~0    2.86 h 100911a_k2  98000   Tau A / CGP transit (Sat AM)
10 100912  2348  B4  258 ----- 38.00 103 s  ~0    2.86 h 100912a_k2  98000   Overnight SDP
10 100913  0636  B4  258 ----- 38.00 103 s  ~0    2.86 h 100913a_k2  98000   Tau A / CGP
10 100914  2340  B4  258 74.56 38.00 103 s  ~0    2.86 h 100914a_k* 196000   Overnight SDP
10 100915  0610  B4  258 74.56 38.00 103 s  ~0    2.86 h 100915a_k* 196000   Tau A / CGP.
10 100915  2336  B4  258 74.56 ----- 103 s  ~0    2.86 h 100915b_k1  98000   Overnight SDP
10 100916  0536  B4  258 74.56 ----- 103 s  ~0    2.86 h 100916_k1   98000   Tau A / CGP
10 100916  2332  B4  258 74.56 ----- 103 s  ~0    2.86 h 100916b_k1  98000   Overnight SDP
10 100917  0528  B4  258 74.56 ----- 103 s  ~0    2.86 h 100917a_k1  98000   Tau A / CGP
10 100918  0524  B4  258 74.56 38.00 103 s  ~0    2.86 h 100918a_k* 198000   Tau A / CGP (Sat AM)
10 100918  2324  B4  258 74.56 38.00 103 s  ~0    2.86 h 100918b_k* 196000   Overnight SDP
10 100919  0520  B4  258 74.56 38.00 103 s  ~0    2.86 h 100919a_k* 198000   Tau A / CGP (Sun AM)
11 100919  2320  B4  258 74.56 38.00 103 s  ~0    2.86 h 100919b_k* 196000   Overnight SDP
11 100920  0516  B4  258 74.56 38.00 103 s  ~0    2.86 h 100920a_k* 196000   Tau A / CGP
11 101010  0404  B4  258 74.56 38.00 103 s  ~0    2.86 h 101010a_k* 196000   Tau A / CGP (Sun AM)
11 101011  0400  B4  258 74.56 38.00 103 s  ~0    2.86 h 101011a_k* 196000   Tau A / CGP
F1 101011  1834  B4  258 74.56 38.00 103 s  ~0   11.44 h 101011b_k* 792000   B1919+21 -> SDP -> TauA/CGP
11 101013  1826  B4  258 74.56 38.00 103 s  ~0   11.44 h 101013_k*  792000   B1919+21 -> SDP -> TauA/CGP
```

Footnotes:

^6 Observed jabbering on Stand 167 at ARX output on Aug 25; remedied. Indicated datasets may have been affected.

First column ("d") refers to the USB external hard drive at VT that the data has been archived to:
"1","2" means "iomega1","iomega2", and so on; "F1" is "Fantom1TB".

All times are LWA-1 local time (LT), as kept by the PC doing the collection. "unkn" means "unknown" (probably, "not logged"). k1/k2 are not explicitly s

"Src A" is what the first channel (on k1 and k2) is recording. Similarly for "Src B".
If this is a number, it is a stand (EW pol for Stands 1-256, NS pol for Stand 258).
If the first character is "B", it is beamformer output. Refer to the configuration (i.e., "S60-2d") for details.

"Freq" is center frequency. Note spectrum for channels with center frequency above 60 MHz will have been digitized
in the second Nyquist zone and will therefore be spectrally-reversed.

(A) = Duration of the acquisition represented by each file in the dataset.
This is the contiguous "time on the sky" represented by each file.

(B) = Time gap between files, denoted as follows:
  ~0: Nearly contiguous; Next file starts as soon as the previous one ends; probably within milliseconds.
       Timestamps written into filenames may be useful in time-aligning files, if desired.
   5: File start times separated by 5 minutes
   15: File start times separated by 15 minutes

(C) = Duration of experiment; i.e., time from start of first file to start of last file.

"dataset" is name of directory(s) containing observation. "?" usually means "1" and "2".

"MB" indicates the size of the dataset in MB.

References

[1] S. Ellingson, "Sensitivity of Antenna Arrays for Long-Wavelength Radio Astronomy," *IEEE Trans. Ant. & Prop.* , *in press.* Preprint available on-line as Long Wavelength Array Memo 166 (http://www.phys.unm.edu/∼lwa/memos) and as arXiv:1005.4232v1 [astro-ph.IM].

[2] B. Hicks, "LWA FEE, version 1.7 (a)", Long Wavelength Array Engineering Memo FEE0022, May 10, 2009.

[3] S. Ellingson, J. Craig, and J. Hartman, "LWA-1 Antenna Position and Cable Data", Ver. 3, Long Wavelength Array Memo 170, December 9, 2010. [online] http://www.phys.unm.edu/∼lwa/memos.

[4] J. Craig, "Design of the Analog Signal Processor Subsystem for a Long Wavelength Array Station", Long Wavelength Array Engineering Memo ASP0005, Nov. 11, 2009.

[5] Q. Liu and S. W. Ellingson, "FPGA-based Direct Conversion Receiver with Continuous Acquisition to a PC", Virginia Tech Internal Report, July 13, 2009. Available through the ETA project website, http://www.ece.vt.edu/swe/eta/.

[6] Q. Liu and S. W. Ellingson, "Coherent Dual-Sampling Direct Conversion Receiver with Continuous Acquisition over Ethernet to a PC", Virginia Tech Internal Report, June 1, 2010. Available through the ETA project website, http://www.ece.vt.edu/swe/eta/.

[7] S.W. Ellingson, "Report on VT LWA-1 Site Activity, Jan 7-12, 2010", Long Wavelength Array Engineering Memo SLC0013, Jan 16, 2010. Available online at http://www.ece.vt.edu/swe/lwavt/.

[8] J.W.M. Baars *et al.* (1977), "The Absolute Spectrum of Cas A; An Accurate Flux Density Scale and a Set of Secondary Calibrators", *Astron. Astrophys.*, 61, 99.

[9] B. Hicks *et al.*, "Design of the LWA-1 Array, Antenna, Stand, Front End Electronics, and Ground Screen", May 15, 2009. Document provided as part of the LWA-1 "Long Lead Review", available through the Long Wavelength Array Engineering Wiki.

[10] S.W. Ellingson, "Antennas for the Next Generation of Low Frequency Radio Telescopes", *IEEE Trans. Ant. & Prop.*, Vol. 53, No. 8, August 2005, pp. 2480-9.

[11] S. Ellingson, "A Parametric Model for the Normalized Power Pattern of a Dipole Antenna over Ground", Long Wavelength Array Memo 175, December 8, 2010. [online] http://www.phys.unm.edu/∼lwa/memos.

[12] S. Ellingson, "LWA MCS Sky Model (LMSM) ver. 0.1", LWA Engineering Memo MCS0037, Nov 08, 2010. Available online at http://www.ece.vt.edu/swe/lwavt/.

[13] A. de Oliveira-Costa *et al.* (2008), "A Model of Diffuse Galactic Radio Emission from 10 MHz to 100 GHz," astro-ph/0802.1525.

[14] A. E. E. Rogers, P. Pratap, and E. Kratzenberg, "Calibration of Active Antenna Arrays Using a Sky Brightness Model," *Radio Sci.*, vol. 39, no. RS2023, 2004.

[15] S. Ellingson, "Effective Aperture of a Large Pseudorandom Low-Frequency Dipole Array," Long Wavelength Array Memo 73, Jan 13, 2007. [online] http://www.phys.unm.edu/∼lwa/memos.

[16] J. Hartman, "Antenna Pattern Measurements from a Two-Element Interferometer," Long Wavelength Array Memo 155, Apr 15, 2009. [online] http://www.phys.unm.edu/∼lwa/memos.